Function Follows Form:

How Connectivity Patterns Govern Neural Responses

by

David Eugene Osher

B.Sc. Psychology
The Ohio State University 2006

SUBMITTED TO THE
DEPARTMENT OF BRAIN AND COGNITIVE SCIENCES
IN PARTIAL FULFILLMENT OF THE REQUIREMENTS FOR THE DEGREE OF

DOCTOR OF PHILOSOPHY IN NEUROSCIENCE
AT THE
MASSACHUSETTS INSTITUTE OF TECHNOLOGY
June 2013

© David E. Osher, MMXIII. All rights reserved

The author hereby grants to MIT permission to reproduce and distribute publicly paper and electronic copies of this thesis document in whole or in part in any medium now known or hereafter created.

Author.....
David E. Osher
Department of Brain and Cognitive Sciences
May 3, 2013

Certified by.....
John D. E. Gabrieli
Grover Hermann Professor in Health Sciences, Technology and Cognitive Neuroscience
Thesis Supervisor

Accepted by.....
Matthew A. Wilson
Sherman Fairchild Professor of Neuroscience
Director of Graduate Education for Brain and Cognitive Sciences

Function Follows Form:

How Connectivity Patterns Govern Neural Responses

by

David Eugene Osher

Submitted to the Department of Brain and Cognitive Sciences
on May 3 2013, in partial fulfillment of the
requirements for the degree of
Doctor of Philosophy in Systems Neuroscience

Abstract

Connectivity restricts and defines the information that a network can process. It is the substance of information processing that underlies the patterns of functional activity in the brain. By combining diffusion-weighted imaging or DWI, with fMRI, we are able to non-invasively measure connectivity and neural responses in the same individuals and directly relate these two measures to one another. In Chapter 2, I first establish the proof-of-principle that anatomical connectivity alone can predict neural responses in cortex, specifically of face-selectivity in the fusiform gyrus. I then extend this novel approach to the rest of the brain and test whether connectivity can accurately predict neural responses to various visual categories in Chapter 3. Finally, in Chapter 4, I compare and contrast the resulting models, which are essentially networks of connectivity that are functionally-relevant to each visual category, and demonstrate the type of knowledge that can be uncovered by directly integrating structure and function.

Thesis Supervisor: John D. E. Gabrieli
Title: Grover Hermann Professor in Health Sciences and Technology and Cognitive Neuroscience

----BLANK PAGE---

Contents

Acknowledgements

First and absolutely foremost I want to acknowledge and appreciate my lifelong colleague and collaborator, Zeynep Saygin. Without her, none of this could have been possible. Without her, the ideas and methods expressed in this thesis could never be realized. My own interest in brain connectivity is doubtlessly due to Zeynep. I began my graduate career researching visual attention, and Zeynep's interest in connectivity proved to be remarkably infectious. It wasn't long before we joined forces, and together we accomplished so much in such a short time. Much of this can be attributed to her direction, organization, and truly ingenious insight. Zeynep is able to comprehend anything with extraordinary speed and in any domain, be it abstract mathematics or novel analytics. Her unending gifts are especially manifest in her ability to perceive a research project holistically, and rapidly solve problems along the way. Besides, we work so beautifully together that our research progressed with prodigious ease. Zeynep has made the labor of graduate school surprisingly wonderful, and has always been my utmost champion, standing by my side when I needed her most. She is an incredible leader, a brilliant thinker, a dedicated teacher, a fiercely loyal friend, and now my loving spouse. I would be satisfied enough only to work beside her, but I am lucky: I get to share my entire life with her, and this fills my heart with overwhelming pride.

I also thank John Gabrieli for being such a fantastic mentor. John possesses the perfect balance as an advisor: he is always there for you, readily available when you need him, and never overly demanding or pushy. I especially thank him for helping me to develop and flourish in his lab by giving me the independence, resources, and guidance that were absolutely essential in making this thesis possible.

Next, I'd like to thank Rebecca Saxe. Her advice and enthusiasm has been critical to these projects. She has also been a great friend and mentor, and is always there to listen.

Rebecca's warm and welcoming attitude makes it easy to approach her about anything, and her ability to rapidly conjure solutions to nearly any problem has added an essential perspective on nearly all aspects of this thesis.

Bob Desimone is truly an inspiration to me. I first came across his research as an undergraduate, and I soon found myself devouring any resource I could find about the neuroscience of vision and attention. Throughout graduate school, Bob continued to influence my point of view in neuroscience: early on, he trained me in physiology, and gave me a solid systems-level perspective on the brain, from cell to network.

I thank Bruce Fischl, who is one of the most responsive and capable scientists that I have worked with. His technical prowess is simply unmatched. You'd be surprised by how quickly he can come up with the next best analysis.

I also thank Kami Koldewyn, Nancy Kanwisher, and easily *every* member of the Gabrieli, Desimone, and Kanwisher labs. Finally, I thank my parents, Sylvia and Peter, and my siblings, Paul and Julia; each has been an endless source of support and encouragement for following my dreams.

for Zeynep

Chapter 1

Introduction.

Connectivity is among the most important of structural elements, since it restricts and defines the sort of information that a network can process; it is the substance of information processing that links functional activity to the physical mechanics that generate it. To explain brain function, it is consequently of great priority that neuroscientific research discover the relationship between neural response patterns and the connections that produce and relay them.

Since the 19th century, neuroanatomists have been passionate about the study of connectivity. Fiber bundles were painstakingly characterized, and after the advent of the Golgi stain, individual neuronal processes were scrupulously mapped. In the early 1960s, Hubel & Wiesel laid the groundwork for some of the most fundamental concepts of cortical processing of vision (Hubel and Wiesel, 1962). Their legacy as experimentalists casts a shadow over their impact on computational neuroscience: they suggested connectionist models that offered explanatory accounts of their findings. While they certainly were not the first to do this, their models remain influential and continue to inspire and sculpt new generations of neuroscientists.

Most explanatory accounts of brain function have almost always been purely theoretical, rather than directly data driven, in that they combine reports from disparate anatomical and functional studies. To fully realize the relationship between structure and function, it is important to assess both measures within the same brain, such that the functional characteristics of neural

units (e.g. neuroimaging voxels or electrophysiological units) can be precisely aligned to their connective relationships.

The first attempts to directly link structure to function came about after the development and refinement of approaches that allowed intracellular recordings of single units followed by injections of horseradish peroxidase (HRP) into those neurons to trace their connections and by this, explain their function. Gilbert and Wiesel, after describing the horizontal connections of primary visual cortex (V1) pyramidal cells (Gilbert and Wiesel, 1979), went on to use such a technique to demonstrate that these connections specifically innervate columns with similar orientation preferences (Gilbert and Wiesel 1983, 1989). This result has been shown using various approaches in several species, such as optical imaging and axonal tracing in the tree shrew (Bosking et al. 1997; also see Martin et al. 2002; Lee and Reid 2011 for reviews). Furthermore, by linking receptive field information with connectivity, Mooser et al. were able to demonstrate how axonal targeting of non-orientation selective units (V1 cells that receive LGN input) are able to generate orientation-selective units in superficial layers of V1 by means of their connectivity patterns (Mooser et al. 2004). More recently, impressive combinations of two-photon microscopy (for assessing function) and serial electron microscopy (for visualizing connectivity) have helped delineate the functional roles of inhibitory and excitatory connectivity patterns in V1 and the retina that generate direction-selectivity (Bock et al. 2011; Briggman et al. 2011).

These approaches have mainly focused on intra-areal connectivity patterns due to technical limitations. A very recent study used two-photon imaging of V1 axons arriving at higher-level visual cortices to show that V1 projections specifically innervate cells with similar visual preferences (Glickfeld et al. 2013). These studies are amazing technological feats and

provide the foundation of our current understanding of how structure determines function in the brain. However, these techniques can measure only a portion of the connectivity of a region and for simplicity reasons, have focused mainly on feed-forward transformations, which must be only a part of the whole picture. Much of the brain is massively interconnected, and so in order to have a more complete understanding of structure-function relationships, we need to look at the structure and function of the whole brain, with techniques such as magnetic resonance imaging (MRI).

Functional MRI (fMRI) is noninvasive and captures function across the whole brain, and has thus greatly enhanced the field's understanding of human brain function. However, the overwhelming majority of fMRI research is descriptive, yielding results that essentially localize activity patterns to brain regions under specific circumstances (e.g. stimuli, task, populations). In order to advance fMRI research towards mechanistic principles, investigators will need to adopt new approaches that explain neural activity as a function of the underlying neural structures that process information.

Diffusion-weighted imaging (DWI) is a noninvasive neuroimaging technique that measures the propensity of water to travel along myelinated axons. Since the diffusion of water is restricted via myelination, DWI can be used to measure the direction of water diffusion along the length of fiber bundles and thus estimate brain connectivity *in vivo* (Behrens et al. 2003a,b). DWI can be analyzed alongside fMRI data in the same individual. By combining these modern neuroimaging tools and analyzing DWI alongside fMRI data, researchers now have a unique opportunity to link structure and function in the same individual, and move toward establishing anatomical underlying principles of human brain function. In this thesis, I show evidence that structural connectivity as measured with DWI can predict visual representations voxel-wise

across the brain and investigate the structural networks that underlie visual representations in cortex.

Given the assumption that brain structure determines function, functionally distinct regions of cortex should be structurally distinct in their connections to other areas. In Chapter 2, I first test this hypothesis in relation to face selectivity in the fusiform gyrus. By using only structural connectivity, as measured through diffusion weighted imaging, or DWI, one can predict functional activation to faces in the fusiform gyrus. By showing that the neural response of each voxel (e.g. its face-selectivity) can be predicted from the extrinsic structural connectivity between that voxel and each of the other brain regions, we demonstrated that unique voxel-wise connectivity fingerprints determine face-selectivity in the fusiform. These predictions outperformed two control models and a standard group-average benchmark. The structure-function relationship discovered from these participants was highly robust in predicting activation in a second group of participants, despite differences in acquisition parameters and stimuli. This approach can thus reliably estimate activation in participants who cannot perform functional imaging tasks, and is an alternative to group-activation maps. Additionally, we identified cortical regions whose connectivity is highly influential in predicting face-selectivity within the fusiform, suggesting a possible mechanistic architecture underlying face processing in humans.

In Chapter 3, I extend this method to the whole brain and ask whether connectivity fingerprints are present throughout the cortex for high-level visual categories. We used anatomical connectivity to predict functional activity in each gray matter voxel of the brain. Diffusion-weighted images and fMRI images were acquired from two groups of healthy subjects. Probabilistic diffusion tractography was performed from each anatomically-defined parcel to all

other anatomical parcels. For each parcel, we modeled the fMRI data as a function of connection probability using linear regressions. The models surpassed performance distributions generated from randomly permuted data, indicating that the connectivity data are structured sufficiently for prediction. The models also accurately predicted fMRI activation in new participants in (two different groups) using only their DWI data. Further, connectivity-based predictions also outperformed a group-average benchmark model, both across the whole brain and within each functionally-specific region of interest (fROI), in the two groups of participants. Overall, we found that connectivity patterns account for individual variability and are unique for different functions. These results support the hypothesis that connectivity is predictive of functional specialization at a voxel-wise grain across the cortex, thus confirming and extending a fundamental assumption in neuroscience.

A region's connections are not equally influential for a particular mental function. For example, less than 5% of the inputs to macaque V1 arrive from the optic radiations, which are undeniably critical agents to visual responses in V1 (Peters and Payne 1993; Peters, Payne, and Rudd 1994). Testing whether unique connectivity fingerprints exist and determine function will only be the first step in identifying the critical connections that underlie function. Thus, after discovering which of the tasks/stimulus categories possess a meaningful relationship linking connective structure with function, I next investigated what the functionally-relevant connections are and what makes a voxel's pattern of connections unique for one particular function, or general for all visual functions.

In Chapter 4, I explored the functional connectomics for different visual categorical representations. Diffusion-weighted images and fMRI images were acquired from two groups of healthy subjects, and modeled as before (see above). Connectivity models of functional

activation to visual categories were used to identify the subset of connections that best predicted voxel-wise functional activation, or the functionally relevant network (FRN), for each functional contrast for each anatomical parcel. By comparing the FRNs across visual categorical domains, we found that there are unique sets of connections for predicting different functions. We also discovered that object and scene representations shared some aspects of the FRNs with one another, while body and face FRNs were similar to one another yet dissimilar to object and scene FRNs. These results extend previous findings and demonstrate the utility of using anatomical connectivity to predict functional responses to a variety of stimuli, encouraging the assembly of a database of model coefficients for numerous other conditions. Such a database would enable a researcher to estimate functional responses to a range of experimental conditions from a single diffusion scan that lasts only about 10 minutes. Furthermore, amassing information about the relationship between structure and various functional responses will build a "functional connectome", a comprehensive resource of the connectivity patterns that underlie the gamut of brain function.

References.

Gilbert CD & Wiesel TN. Morphology and intracortical projections of functionally characterised neurones in the cat visual cortex. *Nature*. 280:120 –125. (1979).

Gilbert CD, Wiesel TN. Clustered intrinsic connections in cat visual cortex. *J Neurosci* 3:1116 – 1133. (1983).

Gilbert, C. D. & Wiesel, T. N. Columnar specificity of intrinsic horizontal and corticocortical connections in cat visual cortex. *J. Neurosci.* 9, 2432–2442 (1989).

Hubel D.H & Wiesel, T.N. Receptive fields, binocular interaction and functional architecture in the cat's visual cortex." *J.Physiology*, **160**(1): 106-154.2. (1961).

Bosking et al. 1997 Bosking WH, Zhang Y, Schofield B, Fitzpatrick D. Orientation selectivity and the arrangement of horizontal connections in tree shrew striate cortex. *J Neurosci* 17:2112–2127. (1997).

Martin. K.A. Microcircuits in visual cortex. *Curr Opin Neurobiol*, 12, pp. 418–425. (2002).

Lee, W.C., Reid R.C. Specificity and randomness: structure-function relationships in neural circuits. Curr. Opin. Neurobiol., 21, pp. 801–807 (2011).

Mooser, F., Bosking, W.H., Fitzpatrick, D. A morphological basis for orientation tuning in primary visual cortex Nature Neuroscience 7(8), 872-879. (2004).

Bock, D. D. et al. *Nature* 271, 177–182 (2011).

Briggman, K. L., Helmstaedter, M. & Denk, W. *Nature* 271, 183–188 (2011).

Glickfeld, L., Andermann, M., Vincent Bonin & R Clay Reid. Cortico-cortical projections in mouse visual cortex are functionally target specific. Nat Neuro. 2013.

Behrens, T.E., *et al*. Non-invasive mapping of connections between human thalamus and cortex using diffusion imaging. *Nat Neurosci* **6**, 750-757 (2003a).

Behrens, T.E., *et al.* Characterization and propagation of uncertainty in diffusion-weighted MR imaging. *Magn Reson Med* **50**, 1077-1088 (2003b).

Peters, A., & Payne, B. R. Cereb. Cortex. 3, 69 (1993).

Peters, A., Payne, B.R., Rudd, J. Cereb. Cortex. 4, 215 (1994).

Chapter 2

Anatomical connectivity patterns predict face-selectivity in the fusiform gyrus.

Parts published as:

Saygin Z.M.*****, Osher D.E*, Koldewyn K., Reynolds G., Gabrieli J.D.E., Saxe R.R. Anatomical connectivity patterns predict face-selectivity in the fusiform gyrus. (Nature Neuroscience 2012).

Abstract: A fundamental assumption in neuroscience is that brain structure determines function. Accordingly, functionally distinct regions of cortex should be structurally distinct in their connections to other areas. We tested this hypothesis in relation to face selectivity in the fusiform gyrus. By using only structural connectivity, as measured through diffusion weighted imaging, we are able to predict functional activation to faces in the fusiform gyrus. These predictions outperformed two control models and a standard group-average benchmark. The structure-function relationship discovered from these participants was highly robust in predicting activation in a second group of participants, despite differences in acquisition parameters and stimuli. This approach can thus reliably estimate activation in participants who cannot perform functional imaging tasks, and is an alternative to group-activation maps. Additionally, we identified cortical regions whose connectivity is highly influential in predicting face-selectivity within the fusiform, suggesting a possible mechanistic architecture underlying face processing in humans.

Introduction

A fundamental assumption in neuroscience is that function is deeply-rooted in anatomical structure, such as extrinsic connectivity. A region's connectivity pattern determines both the information available as inputs from other regions, and its output and influence on other areas. Indeed, changes in connectivity have been shown to occur at the boundaries of functionally-defined regions that can be identified through cytoarchitectonics (supplementary motor area (SMA) vs. pre-SMA)[1]. If anatomical connectivity is important for functional operations, then variation in connectivity should correspond with and predict variation in function, even in regions that are currently not anatomically definable or spatially consistent across the population. This intuitive claim has not yet been formally explored, though various frameworks for such an analysis have been suggested[2].

In the absence of any additional information, can structural connectivity accurately predict the location and degree of the functional response in the brain? The extrinsic connectivity pattern of a structure may contain sufficient information to predict the extent to which each voxel will respond to a given functional contrast. This hypothesis could be tested using a functional contrast that consistently elicits robust responses, and constrained to an anatomical structure that reliably encapsulates such responses across participants, even if they vary spatially within the region.

Regions involved in face-processing may be well-suited for directly testing this conjecture, given their posited specificity of function and replicability across brain imaging techniques, participants, and species. A dedicated network of brain regions has been consistently reported to selectively respond to faces, as revealed by fMRI[3, 4], single-unit recordings[5, 6], and microstimulation[7]. The most robust and selective component of this network is within the

fusiform gyrus[8], in a functionally defined region that is selectively activated in response to faces relative to objects[9] or scenes[10]. This region is typically larger and more reliably observed in the right fusiform, and is known as the fusiform face area (FFA). This is consistent with a wide range of evidence that most aspects of face perception are right-hemisphere dominant in the human brain[8, 11, 12]. Further, damage to the right fusiform disproportionately impairs face recognition, sometimes even without disturbing other stimulus categories[13, 14]. Given that it is the right fusiform that best responds to faces across participants (e.g.[8, 15]), we chose this region as a testing ground for modeling brain activity as a function of structural connectivity.

A purely structural substrate of face-selective cortices has not yet been established, possibly due to complications in relating classic approaches of connectivity (such as histological tract-tracing) with functional localization in the same individual. However, diffusion weighted imaging (DWI), an MRI technique that measures the propensity of water to travel along myelinated axons, can be used to estimate brain connectivity *in vivo*[16, 17], which can be analyzed alongside fMRI data in the same individual. Using a probabilistic tractography algorithm, we defined the connection probability of each right fusiform voxel (seeds) to all other anatomically parcellated regions (targets) (see **Supplementary Fig. 1,2** for exemplar pathways[18-20]). For the same participants, the functional activation of faces relative to scenes for each voxel in the fusiform was calculated. We then analyzed the relationship between functional activation in the fusiform and its connection probabilities with the rest of the brain, through a multivariate, voxel-by-voxel approach. This approach allowed us to directly test the conjecture that while the locations of face-selective voxels are variable across the population, their extrinsic connections vary systematically with function in each individual, such that the connection patterns alone can predict functional activation.

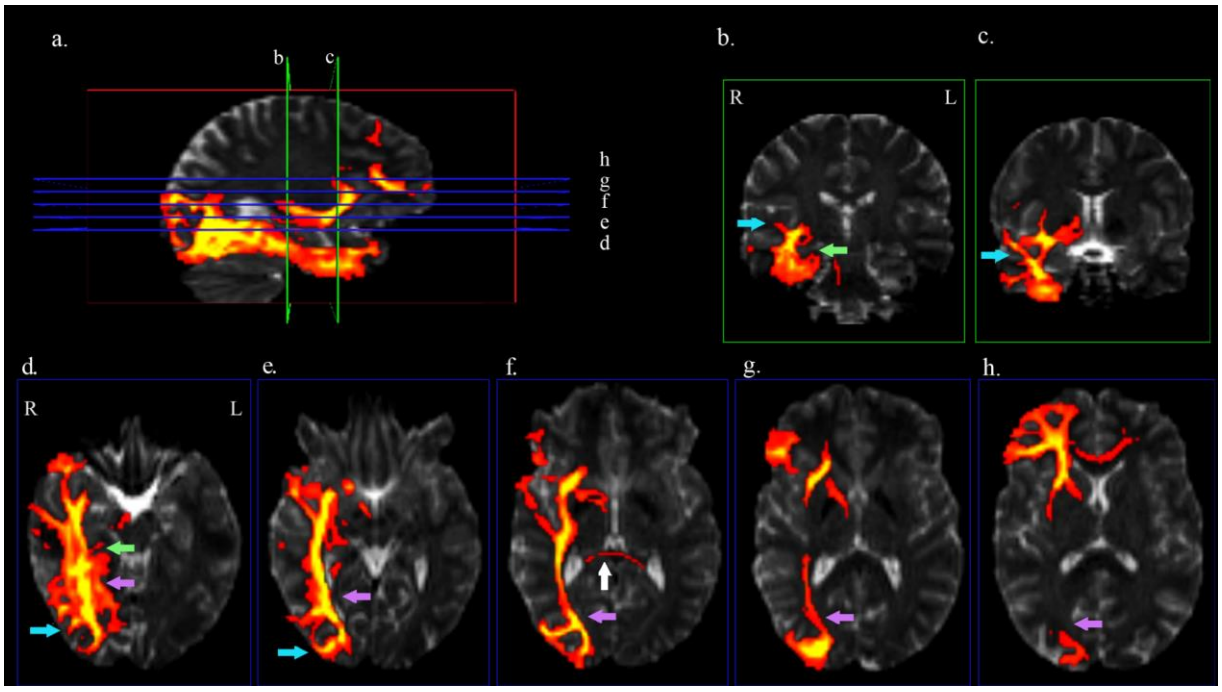

Supplementary Figure 1. Probabilistic tracts for an example subject, overlaid on the same subject's low-b diffusion images. These depict all possible tracts that the tractography algorithm used to connect the fusiform directly or indirectly with other brain regions. These tracts are naïve to functional selectivity in the fusiform. **a.** Right sagittal section showing the inferior longitudinal fasiculus (ILF), which travels inferiorly to the uncinate, as well as the superior longitudinal fasiculus (SLF), and short/U-fibers. It also displays the slice locations for coronal slices (green boxes; **b** and **c**) and axial slices (blue boxes; **d** through **h**). The fibers of the inferior longitudinal fasiculus (ILF; purple arrows in **d** through **h**) run anteriorly, connecting the lateral occipital cortex, lingual and fusiform gyri. The ILF then projects laterally to superior, middle, and inferior temporal gyri, and medially to the parahippocampal gyrus (green arrows in **b** and **d**). The forceps major connects the left and right medial cortices (white arrow in **f**) while the U-shaped fibers (blue arrows in coronal sections **b** and **c**; axial sections **d** and **e**) are lateral to the ILF and connect adjacent gyri of the lateral occipito-temporal cortex.

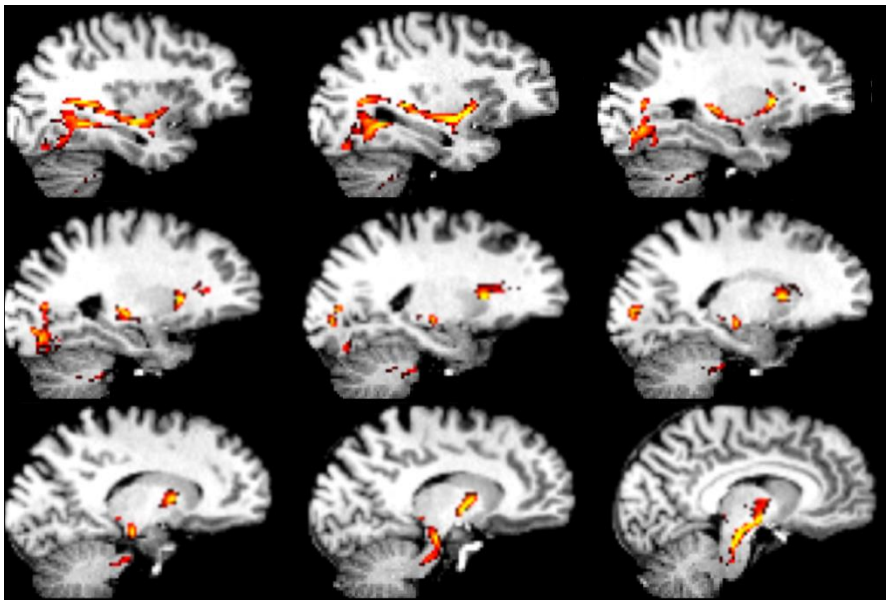

Supplementary Figure 2. Probabilistic tracts overlaid on the subject's anatomical image that was registered to the diffusion images. The sagittal sections on the right hemisphere show possible multisynaptic pathways that the probabilistic algorithm takes from extrastriate cortex, through the pons, and to the cerebellar pathways.

Specifically, a least-squares linear regression was used to model the relationship between each fusiform voxel's connection probabilities and its functional activation by using a leave-one-subject-out cross-validation approach, or LOOCV (**Fig. 1a)**. The resulting model was then applied to the remaining participants' connectivity data, and prediction accuracies were tested against two control models and a benchmark model built from a functional group-average. The group-average is commonly used as a way to build face-selective ROIs in fMRI studies[21], and thus provides a standard that a connectivity-based method should meet. The control models, designed from random permutations and Euclidian distance (see **Methods**), were implemented to evaluate against potential confounds.

In order to assure that the model is not overly fit to the population it was built from, it is good practice to design a model built from all the participants in the LOOCV, and apply it to a separate pool of observations naïve to the model-building procedure[22]. We applied such a model to an independent group of participants from a separate study. This second group provided further examination of the generalizability of the models, since their data were acquired with different DWI scan parameters and a different functional task from the first group of participants.

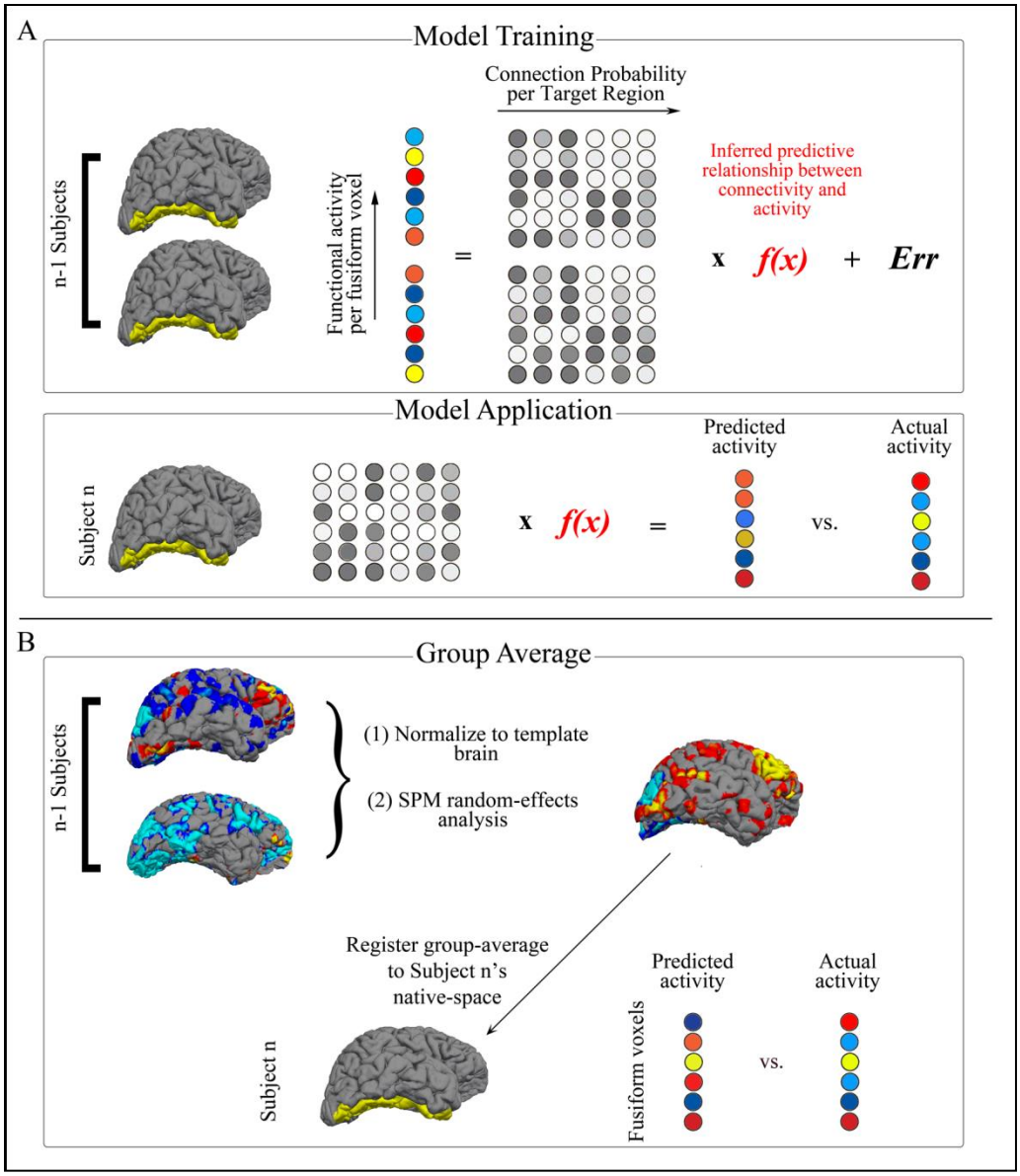

Figure 1 Schematic model design.

(**a**) Linear regression models were trained on all but one participant's data in Group 1. The 22 participants' fMRI data for each voxel in the fusiform gyrus are depicted by circles that are color-coded from red to blue, representing their responses to the contrast of Faces >Scenes). Each voxel's corresponding connection probabilities (for the connectivity model) or Euclidian distances (for the distance model) to each target brain region are depicted by the grayscale

circles. The fMRI data and connectivity or distance data from each fusiform voxel for the 22 participants are used to train the model, and the resulting model, ***f(x)***, is applied to the remaining participant's connectivity or distance data, resulting in predicted fMRI values for each fusiform voxel. The predicted values are then compared to that participant's observed fMRI values and the mean absolute error (MAE) is calculated for each participant. The LOOCV is done iteratively through all the participants, such that each participant has a predicted fMRI image based on a regression from all the other participants. (**b**) Similarly, a LOOCV procedure was also performed for the group-average model, but rather than training a linear regression, each participant's whole-brain fMRI data was spatially normalized into MNI space, superimposed to create composite maps, and a t-static image was generated for the random-effects analysis. This image was registered to the remaining participant's native-space, and only the fusiform gyrus was extracted. This predicted activation based on a group analysis was then compared to that participant's observed activation, and an MAE was computed per voxel.

Methods

Participants

For Group 1, twenty-three participants were recruited from the greater Boston area between the ages of 19 and 42 (mean age = 27.9 ± 1.06, 12 female). Group 2 included twenty-one participants between the ages of 19 and 44 (mean age = 26.9 ± 1.45, 13 female) and were similarly recruited. Both groups of participants were screened for history of mental illness and were compensated at $30/hr. The studies were approved by the Massachusetts Institute of Technology and Massachusetts General Hospital ethics committees.

Acquisition parameters for Group 1

DWI data were acquired using echo planar imaging (64 slices, voxel size 2×2×2mm, 128×128 base resolution, diffusion weighting isotropically distributed along 60 directions, b-value 700s/mm^2) on a 3T Siemens scanner with a 32 channel head-coil[42]. A high resolution (1mm^3) 3D magnetization-prepared rapid acquisition with gradient echo (MPRAGE) scan was acquired on these participants.

We acquired event-related fMRI data (gradient echo sequence TR/TE/flip/volumes/voxel size = 2000ms/30ms/90º/324/3.1×3.1×4mm) while the same participants viewed color images of faces or scenes while performing a 1-back task by responding each time a stimulus repeated. Face stimuli[43] consisted of neutral and emotional faces (angry, disgusted, and happy). Scene stimuli were all neutral outdoor and indoor scenes[44] (http://cvcl.mit.edu/database.htm). Face and scene stimuli were ordered using optseq2[45] (http://surfer.nmr.mgh.harvard.edu/optseq), an optimization program for jittering trials in event-related experiments.

Acquisition parameters for Group 2

DWI acquisition parameters for Group 2 were different, with 30 directions of diffusion, 64 slices, voxel size 2×2×2mm, 128×128 base resolution, b-value 700s/mm^2, but were acquired on the same scanner with the same 32 channel head-coil as Group 1. A high-resolution (1mm^3) 3D magnetization-prepared rapid acquisition with gradient echo (MPRAGE) scan was also acquired on these participants.

Stimuli for the functional MRI consisted of 3-second movie clips of faces, bodies, scenes, objects, and scrambled objects. Movies of faces and bodies were filmed against a black background, and framed to reveal just the faces or bodies of seven children, shown one at a time. Scenes consisted primarily of pastoral scenes filmed through a car window while driving slowly through the countryside or suburb. Objects were selected specifically to minimize any suggestion of animacy of the object itself or of an invisible actor pushing the object. Scrambled object clips were constructed by dividing each object movie clip into a 15×15 box grid and spatially rearranging the location of each of the resulting boxes. Pilot testing indicated that a contrast of the response for moving faces versus moving objects identified the same FFA as that identified in a standard static localizer. Further studies in adults show that the FFA responds similarly to movies of faces as to static snapshots of faces[46].

Functional data were acquired over four block-design functional runs (gradient echo sequence TR/TE/flip/volumes/voxel size = 2000ms/30ms/90º/234/3×3×3mm). Each functional run contained three 18-second fixation blocks at the beginning, middle, and end of the run. During these blocks, a series of six uniform color fields were presented for three seconds each. Each run additionally contained two sets of five consecutive stimulus blocks (faces, bodies, scenes, objects, or scrambled objects) sandwiched between these rest blocks, resulting in two

blocks per stimulus category per run. Each block lasted 18 seconds and contained six 3-second movies clips from each of the five stimulus categories. The order of stimulus category blocks in each run was palindromic and specific movie clips were chosen randomly to be presented during the block. Participants were asked to passively view the stimuli.

fMRI analysis

For Group 1, functional neuroimaging data were analyzed using Statistical Parametric Mapping software (SPM8, Wellcome Department of Cognitive Neurology, London, UK). Preprocessing included slice timing correction, motion correction and linear trend, and temporal filtering with a 128s cutoff. The images were not spatially normalized. Statistical parametric maps (SPMs) of BOLD activation were created using a multiple regression analysis, with regressors defined for the five stimulus categories (neutral, angry, disgusted, happy faces, and scenes). Boxcar functions for each trial type were convolved with a canonical double-γ hemodynamic function (SPM8, www.fil.ion.ucl.ac.uk/spm) to generate each regressor. The resulting maps were spatially smoothed with a 6-mm Gaussian kernel (FWHM), and the t-statistic image was generated per participant for the contrast of Faces>Scenes.

Group 2's data were analyzed with FSL software (www.fmrib.ox.ac.uk/fsl/). Image preprocessing was similar to Group 1: images were motion corrected, smoothed (5mm FWHM Gaussian kernel), detrended, and were fit using a γ function ($\delta = 2.25$ and $\tau = 1.25$). Data were not spatially normalized. Statistical modeling was then performed using a GLM on the preprocessed functional images. Next, t-maps corresponding to the contrast of interest for Faces>Scenes was overlaid on each participant's high-resolution anatomical image.

For both groups, each participant's functional image for the Faces>Scenes contrast was registered to his/her diffusion-weighted image. Because we were interested in predicting relative activation values which were independent of task-specific parameters such as the degrees of freedom, we standardized the T-statistic values (x) across the fusiform gyrus per participant. This detrending was performed for each participant j, such that the mean value in the fusiform was subtracted from each voxel's fMRI value (x_{ij}) and divided by the standard deviation:

$$x_{zij} = \frac{x_{ij} - mean(x_j)}{std(x_j)}$$

The standardized value per fusiform voxel (x_{zij}) of participant j was then used for the subsequent regression models.

Tractography

Automated cortical and subcortical parcellation was performed with FreeSurfer[47, 48] to define specific cortical and subcortical regions in each individual's T1 scan, based on the Desikan-Killiany atlas[49]. Automated segmentation results were reviewed for quality control, and were then registered to each individual's diffusion images, and used as the seed and target regions for fiber tracking. The resulting cortical and subcortical targets were then checked, and corrected for automatic parcellation/segmentation errors if necessary. There was one seed region per participant, and the 85 target regions were defined as all other automatic parcels, not including the seed. The principal diffusion directions were calculated per voxel, and probabilistic diffusion tractography was carried out using FSL-FDT[17, 50] with 25,000 streamline samples in each seed voxel to create a connectivity distribution to each of the target regions, while avoiding a mask consisting of the ventricles.

Regressions

All analyses were performed on subject-specific anatomy, rather than extrapolation from a template brain, except for the group-average models. It is important to note that for the regression models, each observation was an individual voxel in native-space and there was no identifying or matching of spatial location of voxels across participants. Further, the model was blind to the participant each voxel belonged to.

On Group 1, we built a regression model using a leave-one-subject-out cross-validation (LOOCV): the model was trained to predict the standardized fMRI value for each native-space fusiform voxel based on connectivity data concatenated across 22/23 participants, and tested using the remaining participant's data (**Fig. 1a**). This was performed iteratively for all participants. For Group 2, the analyses were performed in a similar manner, except that the regressions were performed on all the participants in Group 1 (23/23), and simply applied to each participant in Group 2's connectivity data to produce an fMRI image of predicted activation. This was then compared to the participants' own observed fMRI images, and MAE's were calculated.

Using the same LOOCV method, we trained a regression model to predict T-values of fusiform voxels based on each voxels' physical Euclidian distance to each other target region's center-of-mass, rather than each voxel's connection probability to each target region. In this way, both the connectivity and distance models had the same number of dimensions, and were generated identically except for the information present in each model. We also considered other 85-dimensional spatial metrics, such as distance to the nearest voxel of each target, and found that these measures were highly similar to the present one. We applied the regression

coefficients from the distance model generated from all Group 1 participants to each participant in Group 2, as described for the connectivity model.

We created random distributions by training models using the observed fMRI images and connection probabilities, but by randomizing the voxel data. We permuted across 5000 random combinations of connection probability to fMRI activation values per participant, and thus obtained a distribution of random MAE per participant. We then performed a one-tailed t-test to determine if the mean of the participant's random distribution was significantly greater than the same participant's MAE for connectivity-based predictions.

Each participant's functional data were spatially normalized into MNI space with FSL and FreeSurfer, checked and corrected for registration errors, and superimposed to create composite maps. For Group 1 cross-validation, we performed LOOCV: a random effects test on whole-brain fMRI data was performed with SPM8 on the contrast images for Faces>Scenes from all but one participant. The resulting t-statistic image, which was based on all the other participants in normalized space, was applied to the participant left out of the group analysis, and registered back into his/her native-space. We analyzed only the right fusiform gyrus in comparing what the group-average predicted to that participant's actual fMRI image using measures of MAE (**Fig. 1b**).

For Group 2, we created the group-average fMRI image using the same method above, but from all Group 1 participants' observed (actual) fMRI images. This fMRI image was mapped on to each participant in Group 2's native-space coordinates, and compared to that participant's observed fMRI pattern.

Accuracy and benchmark comparisons

As a measure of accuracy, we measured the absolute error per voxel (AE, reported in standardized units, s.u.) per participant, by calculating the absolute difference between the predicted and actual values. To statistically compare the performance of the connectivity model to the random and benchmark models, we performed a pairwise t-test per participant across all their fusiform voxels. A criterion threshold of $P < 0.001$ was used to report the number of participants whose activation pattern was better predicted by one model versus another. Mean absolute error (MAE) was also calculated per participant for each model by averaging the AE across the fusiform voxels. A two-tailed Student's t-test of the MAE's per participant was then used to compare models, with the same threshold ($P < 0.001$) to decide which model's predictions were significantly better.

Spatial relationship of function and connectivity

We registered the connectivity data for the right inferotemporal and lingual targets to the native-space anatomical image of each participant in Groups 1 and 2, and projected these data to each participant's native surface vertices using FreeSurfer. The functional data were similarly projected to the surface. We calculated the center-of-mass for the targets with respect to a reference frame fixed at the center-of-mass for each participant's fusiform gyrus (also on the surface). After partitioning the functionals into positive and negative values, we similarly calculated their centers of mass with respect to the fusiform. We observed more subject variability in the medial-lateral dimension for the positive, and anterior-posterior variability for the negative functionals, and therefore calculated correlations between functional values and connectivity strengths along those dimensions respectively. Since both functional and

connectivity centers of mass were calculated with respect to the subject's own fusiform, the correlations were not biased by cross-subject variability in the boundaries between the seed region and the predictive regions.

For the direct analyses of individual subject variation, we registered each Group 2 participant's connectivity data to MNI space, and subsequently onto each other participant's brain, using FreeSurfer and FSL registration tools. We then applied the final model designed from Group 1 to both the original participant's and registered participant's connectivity values. This was done for all combinations of participant pairs (420). We then compared the MAE's from predictions built from each participant's own connectivity with those built from another participant's connectivity across all participants in Group 2. All of the above predictions were restricted to those voxels that overlapped between the original and registered participants.

Results

Comparisons between connectivity and control models

After an initial analysis determined that the data possessed sufficient structure for its use in prediction (**Supplementary Table 1**), we proceeded to build the connectivity models and their controls. A linear regression was trained on the connectivity and fMRI data (faces>scenes) for all participants but one, and the model was applied to the remaining participant's connectivity data to make predictions of this participant's fMRI data in the right fusiform gyrus; this was done iteratively across all participants. We calculated the absolute error (AE) per voxel as the difference between the predicted and actual fMRI images, and mean absolute error (MAE) as a measure of accuracy. **Table 1** summarizes the MAE's for each model.

Supplementary Table 1. Face-selective fusiform voxels have different connectivity patterns than scene-selective voxels. Thirty-four out of eighty-five targets were significantly different across subjects, Bonferonni corrected at $P < 0.05/85$.

Target	p	F
R Inferiortemporal	ε	1194.29
R Lingual	ε	633.70
R Parahippocampal	ε	231.07
R Middletemporal	ε	146.25
R Cerebellum	ε	111.97
R Isthmuscingulate	ε	99.37
R Lateraloccipital	1.22×10^{-15}	65.56
L Inferiortemporal	3.00×10^{-15}	63.64
L Isthmuscingulate	6.41×10^{-13}	52.66
R Hippocampus	9.50×10^{-13}	51.85
R Superiortemporal	1.46×10^{-12}	50.98
R Amygdala	4.44×10^{-12}	48.73
R Precuneus	8.50×10^{-11}	42.76
L Cerebellum	1.25×10^{-10}	41.99
L Hippocampus	2.89×10^{-09}	35.69
L Pericalcarine	1.71×10^{-08}	32.15
L Precuneus	3.52×10^{-08}	30.72
L Cuneus	7.95×10^{-08}	29.11
R Pallidum	1.11×10^{-07}	28.45
R Thalamus	1.69×10^{-07}	27.62
R Cuneus	7.80×10^{-07}	24.62
R Supramarginal	9.95×10^{-07}	24.14
R Parsorbitalis	3.82×10^{-06}	21.52
R Pericalcarine	6.80×10^{-06}	20.40
L Posteriorcingulate	1.12×10^{-04}	15.00
R Ventral diencephalon	1.21×10^{-04}	14.86
R Entorhinal	1.31×10^{-04}	14.70
R Inferiorparietal	1.36×10^{-04}	14.64
R Superiortemporal bank	1.65×10^{-04}	14.27
L Parahippocampal	2.19×10^{-04}	13.73
L Fusiform	2.45×10^{-04}	13.51
R Posteriorcingulate	3.30×10^{-04}	12.95
L Superiorparietal	3.73×10^{-04}	12.72
R Postcentral	4.82×10^{-04}	12.24

* ε indicates double floating point precision, approximately 2.22×10^{-16}

Table 1. Mean absolute error ± s.e. in standard units for voxels in the fusiform gyrus across subjects for models based on connectivity, distance, their mean permutations, and group-average.

	Group 1	Group 2
Connectivity	0.65±0.013	0.68±0.019
Permutation	0.77±0.008	N/A
Distance	1.06±0.066	1.05±0.051
Group-average	0.78±0.031	0.82±0.039

Next, we performed random permutation tests[23] to statistically assess the performance of the connectivity model. We built models designed from the same data but with shuffled pairings between connectivity and functional responses, and by repeating this process 5000 times, we generated a distribution of accuracies from random models for each individual. Relative to this distribution, the connectivity models successfully predicted functional selectivity across voxels in 22 out of 23 participants' fusiform gyri at a threshold of $P < 0.001$.

The distance from a seed voxel to a target region may potentially bias the connection estimates, since local connections are believed to be more probable than distant ones[24, 25]. In addition, the lateral wall of the fusiform gyrus tends to be face-selective while the medial wall more scene-selective. The connectivity model could therefore rely on the relative distance of each voxel to each target, which is basically a high-dimensional spatial coordinate frame. To ensure that the results of the connectivity model were not driven by such unintended relationships, we generated distance control models using the same LOOCV method. These models were designed identically to the connectivity model, with the exception that they used *Euclidian distance* of the fusiform voxels to other brain regions' center-of-mass, rather than their

connectivity. The distance models thus use the same number of predictors as the connectivity models and serve as controls for possible overfitting.

We directly compared the performance of the connectivity and distance models, both across participants (based on MAE) and within participants (based on AE). Across participants, the connectivity model was significantly more accurate than the distance model (two-tailed t-test of connectivity MAE vs. distance MAE, $T(22) = -6.44$, $P = 1.75\times10^{-6}$). A direct comparison of the error per voxel at the individual-subject level revealed that the connectivity-based predictions were significantly different from distance in 21/23 participants at a threshold of $P < 0.001$, all of which were better predicted by connectivity **(Fig. 2a)**.

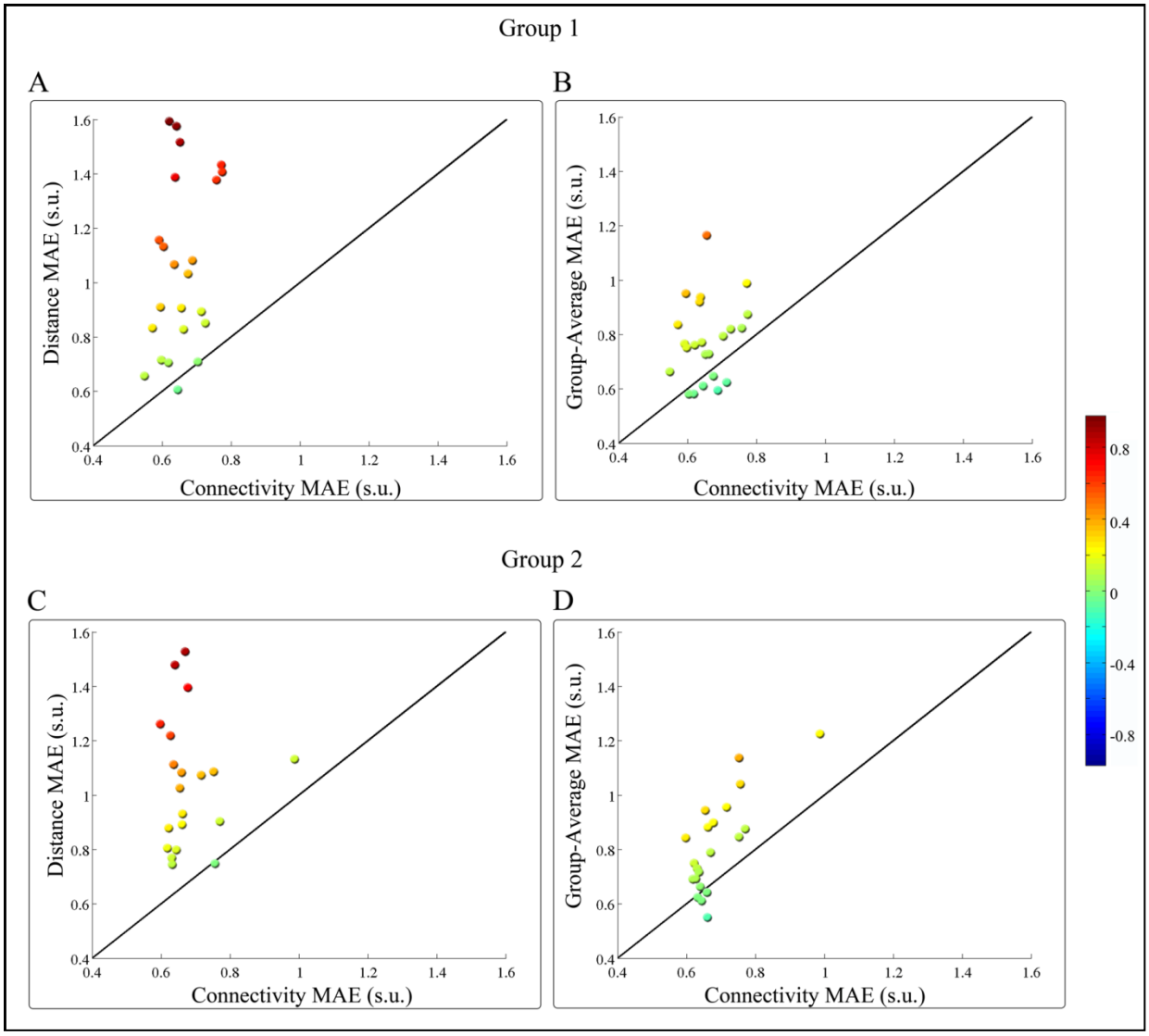

Figure 2 Benchmark comparisons per participant. MAE's from the connectivity-based predictions are plotted against distance or group-average MAE's for each participant. Participants above the unity line thus have higher (worse) MAE's for the benchmark than for the connectivity-based model. Colors reflect the difference between the connectivity-based model and the benchmark; hotter colors indicate better performance of the connectivity-based model. (**a**) For 21/23 participants in group 1, the distance-based predictions had higher (worse) MAE's than connectivity-based predictions, and no participants' functional activation was better predicted by distance than by connectivity. (**b**) The connectivity-based model predicted actual fMRI activation with fewer errors than the group-average for 17/23 participants, while 2 participants' functional activation was better predicted by the group-average than by connectivity.

(**c**) For 18/21 participants in group 2, connectivity-based predictions better predicted actual activations than distance-based predictions, while no participants' functional activation was better predicted by distance than by connectivity. (**d**) 16/21 participants from group 2 had lower MAE's with the connectivity model, while 1 participant had lower MAE's with the group-average model.

Comparisons to group-average models

A group analysis was also performed on the whole-brain fMRI data in an iterative LOOCV fashion: a random effects test was performed on the contrast images for Faces>Scenes for all but one participant (**Fig. 1b**). We registered the resulting group-average to the native anatomical coordinates of the participant left out of the group analysis, and calculated prediction errors for the right fusiform. Since group-analyses are standard in neuroimaging, they were chosen as benchmark models that connectivity-based predictions should meet or exceed in order to be considered useful.

We compared model performance and found that the connectivity-based predictions were statistically better than the group-average, across participants (two-tailed t-test of connectivity MAE vs. group-average MAE, $T(22) = -4.01$, $P = 5.94\times10^{-4}$). The connectivity model was significantly more accurate than the group-average for 17/23 participants at $P < 0.001$, whereas the converse was true for only 2 participants (**Fig. 2b** and **Fig. 3**). For the remaining 4 participants, the models were not significantly different.

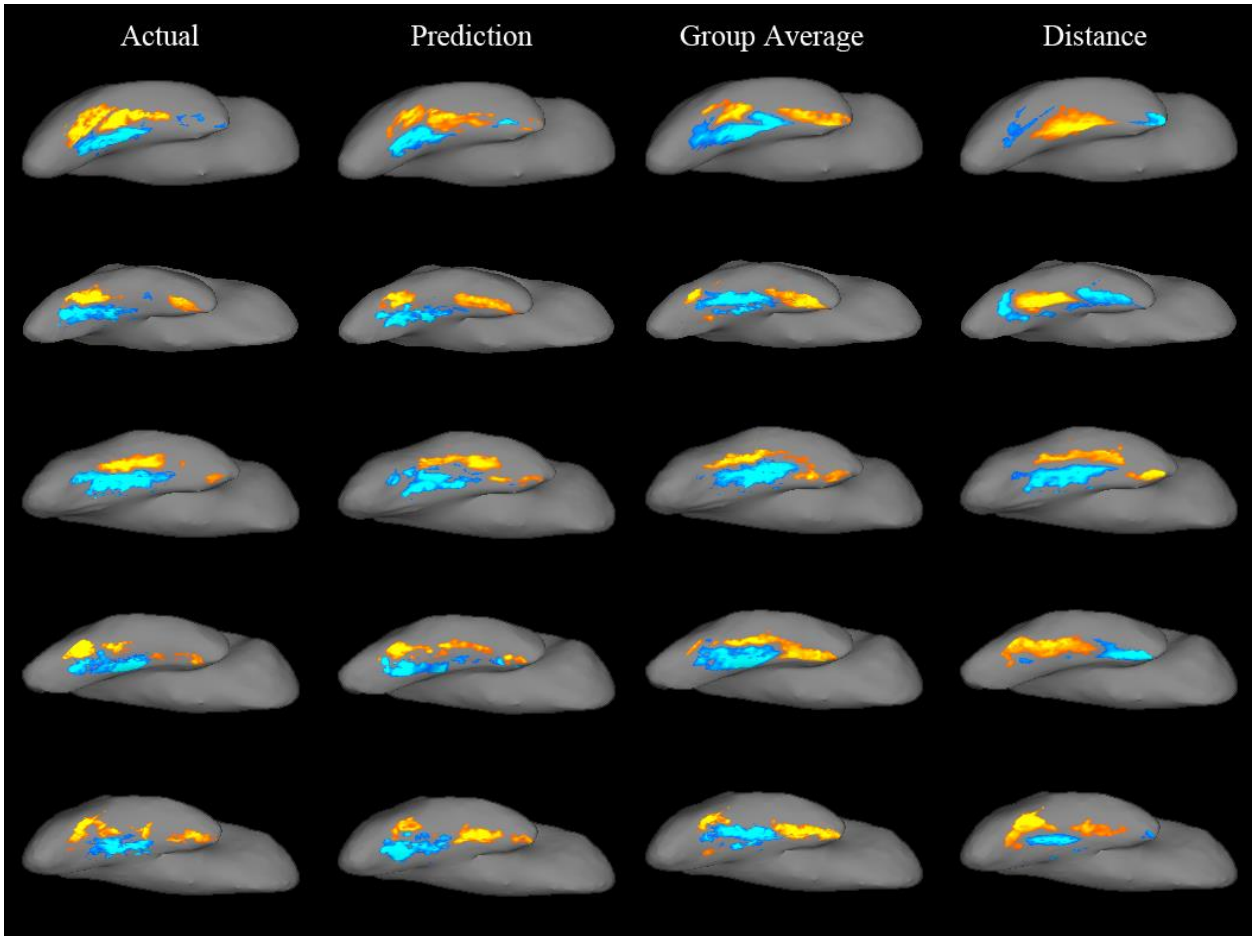

Figure 3 Actual and predicted fMRI activation to Faces>Scenes in the fusiform gyrus of five example participants. For each participant, actual and predicted activation images (t-statistic values for Faces>Scenes) were up-sampled from the DWI structural image (where all the analyses were performed) to the same participant's structural scan, and projected onto the participant's inflated brain surface. Each row is a single participant; the leftmost column displays the actual fMRI activation pattern in the right fusiform gyrus. The remaining columns illustrate, from left to right, predicted fMRI images from: connectivity, group-average, and distance.

Final connectivity models

The connectivity and distance models generated by Group 1 were then applied to a separate group of twenty-one participants, whose connectivity and functional data were naïve to the models. These analyses were performed in a similar manner, except that the regressions were trained on all the participants in Group 1 (23/23), and applied to each participant in Group 2's connectivity data to produce images of predicted activation. We compared these predictions to each participant's observed fMRI image (**Table 1; Fig. 3**). The connectivity model was significantly more accurate across participants than the distance model ($T(20) = –6.72$, two-tailed t-test, $P = 1.53\times10^{-6}$). The connectivity-based predictions were significantly better than distance-based predictions in 18/21 participants at $P < 0.001$ **(Fig. 2c)**. The models were not significantly different for the remaining 3 participants.

A group-average was generated from all participants' contrast images to Faces>Scenes in Group 1 and registered to each participant's own anatomy in Group 2. Across participants, the group-average predictions were significantly less accurate than the connectivity-based predictions ($T(20) = –4.80$, two-tailed t-test, $P = 1.08\times10^{-4}$). Comparing the AE within each participant, we found that functional activation was better predicted by connectivity than by the group-average-based model in 16/21 participants at $P < 0.001$. Only one participant's fusiform profile was more accurately predicted by the group-average than by the connectivity model, and the models were not significantly different for the remaining 4 participants (**Fig. 2d**). The analyses above were repeated for face and scene selectivity in the left fusiform with the same results (**Supplementary Materials**).

In order to investigate which targets made a significant contribution to the final model (**Table 2**), a model built from only those significant predictors (with all other targets' beta

weights set to 0) was applied to the structural connectivity data of Group 2. The MAE across participants was significantly better than the original connectivity model's MAE (new model's MAE = 0.683 ± 0.02; P = 0.038), demonstrating the predictive impact of these regions. Some of the highest positive-predicting regions were right inferotemporal, lateral occipital, and superior temporal, while right lingual and parahippocampal cortices were among the highest negative-predicting regions (**Fig. 4**).

Table 2. List of target regions, along with their coefficients and confidence intervals, which make a statistically significant contribution to the final connectivity model. Positive predictors are listed on the left, negative predictors on the right.

Target	Coefficient	C.I.	Target	Coefficient	C.I.
R inferiortemporal	0.149	0.137 0.161	R lingual	-0.3868	-0.399 -0.375
R lateraloccipital	0.0978	0.085 0.111	R parahippocampal	-0.1373	-0.149 -0.125
R cerebellum	0.0883	0.076 0.1	L fusiform	-0.0638	-0.086 -0.041
R superiortemporal	0.0809	0.062 0.1	R inferiorparietal	-0.0636	-0.081 -0.046
L cerebellum	0.0714	0.05 0.093	L lingual	-0.0634	-0.077 -0.05
L inferiortemporal	0.0635	0.049 0.078	L parahippocampal	-0.0425	-0.058 -0.027
R entorhinal	0.0466	0.036 0.058	L isthmuscingulate	-0.0417	-0.055 -0.028
R middletemporal	0.0293	0.015 0.043	R postcentral	-0.0396	-0.059 -0.02
R parsopercularis	0.0271	0.007 0.048	R isthmuscingulate	-0.0378	-0.051 -0.025
R thalamus	0.0249	0.007 0.043	R lateralorbitofrontal	-0.034	-0.052 -0.016
L pericalcarine	0.0215	0.002 0.041	R parstriangularis	-0.0289	-0.055 -0.002
L middletemporal	0.0199	0.003 0.036	R Hippocampus	-0.0266	-0.041 -0.012
L temporalpole	0.0145	0.002 0.027	L Hippocampus	-0.024	-0.039 -0.009
L lateralorbitofrontal	0.013	0.001 0.025	R caudal anteriorcingulate	-0.0234	-0.043 -0.004
			L superiortemporal	-0.0232	-0.042 -0.004
			R Amygdala	-0.0219	-0.033 -0.01
			L paracentral	-0.0206	-0.033 -0.008
			Brain Stem	-0.02	-0.035 -0.005
			L Amygdala	-0.0152	-0.027 -0.004

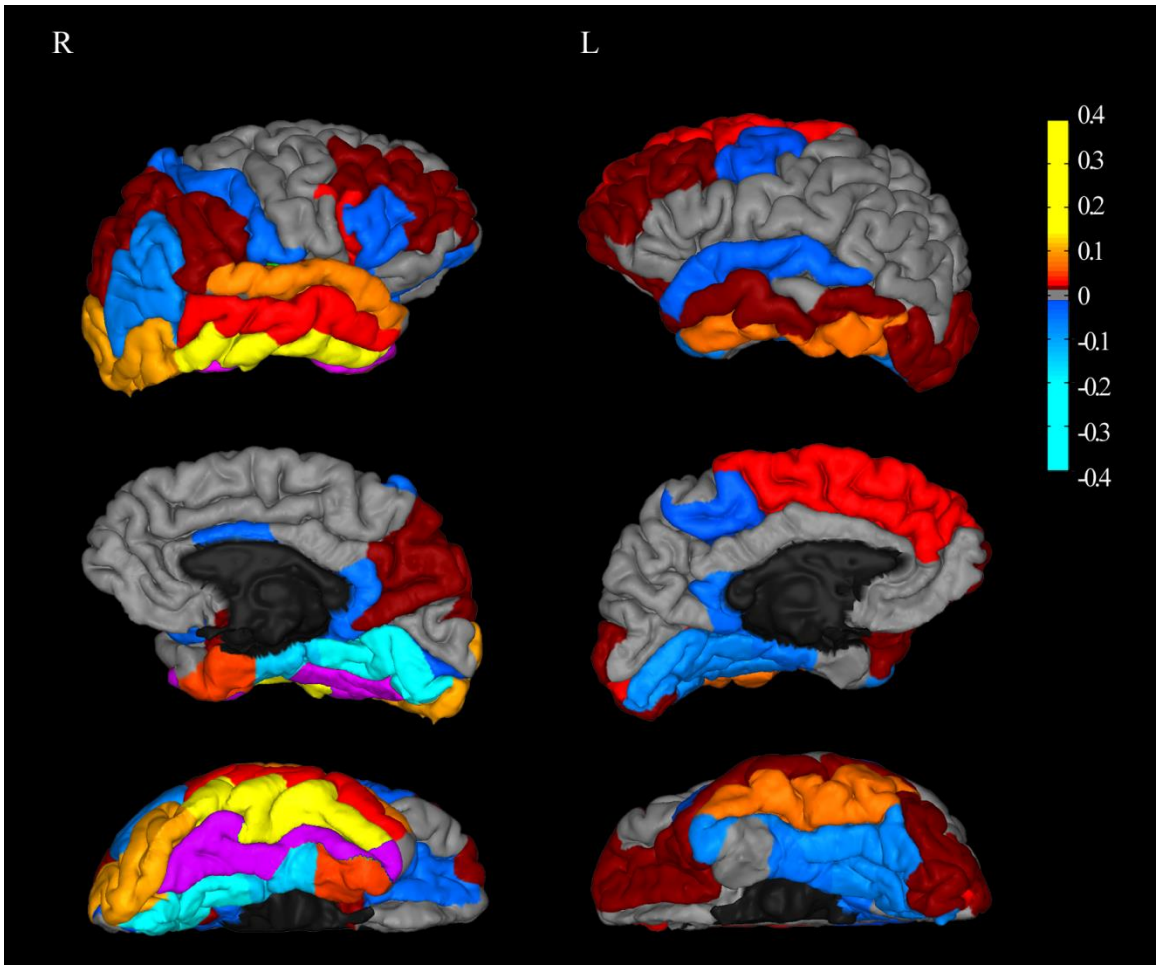

Figure 4 Beta weights for each target region from the final connectivity model. Target regions are color-coded from hot-to-cold to reflect positive or negative beta weight values, and projected to the pial surface of an example participant, with the lateral view on the top row, medial view on the second row, and ventral view on the bottom. The highest predictors of face-selective voxels are regions labeled from red-to-yellow, while the highest predictors of scene-selective voxels are those labeled from blue-to-light blue. The seed region is highlighted in purple. See **Results** for the anatomical nomenclature of the target regions.

Spatial relationship of function and connectivity

We calculated the center-of-mass to the best face (inferotemporal) and scene (lingual) predictors in each participant to visualize the spatial relationship between connectivity and function (**Fig. 5a**). More subject variability was observed in the medial-lateral dimension for the positive, and in the anterior-posterior dimension for the negative functional activation; we therefore calculated correlations between functional values and connectivity strengths along those dimensions respectively. Across participants, centroid locations for face-responses significantly correlated with the centroid locations of connectivity to inferotemporal cortex along the medial-lateral dimension (**Fig. 5b**, $r = 0.46$, $P = 0.002$). That is, individual participants who had a more medial center of functional activation to faces relative to other individuals, also had a more medial center of connectivity to the inferotemporal target region. Similarly, lingual centroids significantly correlated with scene-centroids along the anterior-posterior dimension (**Fig. 5c**, $r = 0.41$, $P = 0.005$).

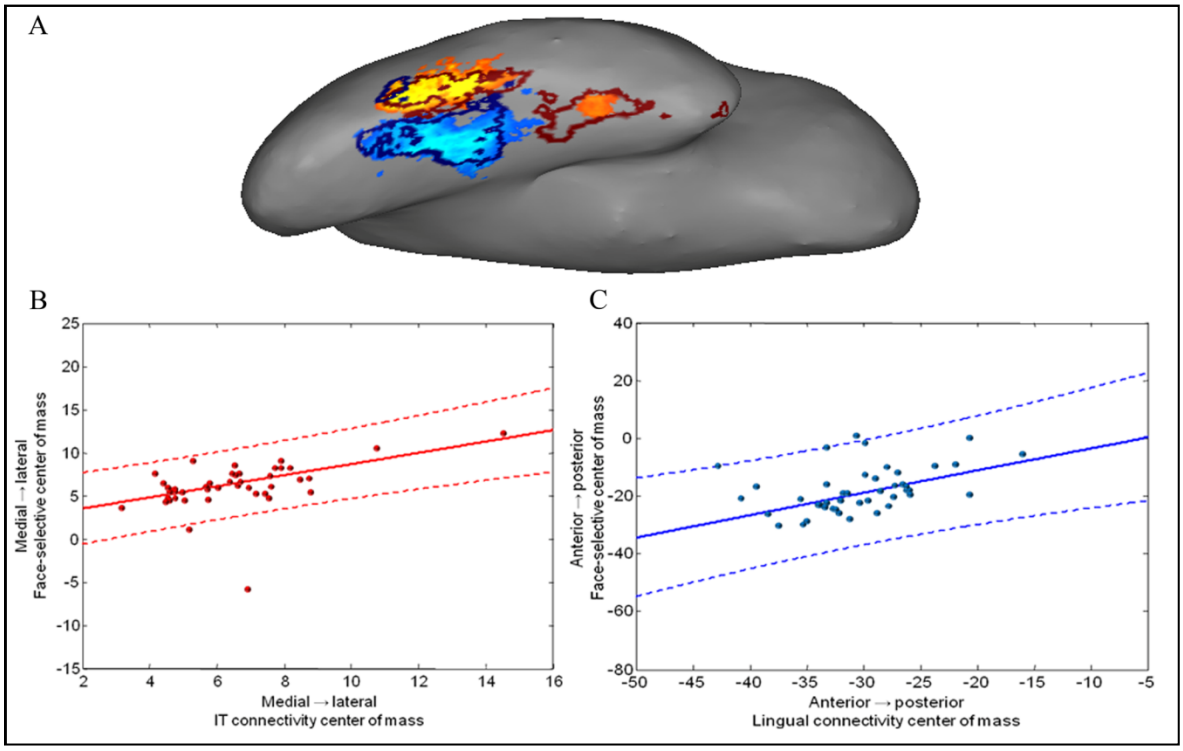

Figure 5 Spatial relationship of function with connection strength to the highest predictors. (**a**) Functional activation of an example participant, with the thresholded boundaries of inferotemporal connectivity overlaid in dark red, and boundaries of lingual connectivity overlaid in dark blue. (**b**) Each participant's center-of-mass of connectivity to inferotemporal is plotted against their center-of-mass of positively-responding voxels, along the medial-lateral dimension, along which each participant's connectivity varies alongside face-selectivity. (**c**) Centroids of lingual connectivity, plotted against centroids of negatively-responding voxels, along the anterior-posterior dimension. Solid lines in **b** and **c** are the least-square fits of these data, and dashed lines are their 99% confidence intervals.

To better establish how individual subject variability in connectivity profiles can be sensitive to individual subject variability in functional responses, we tested whether connectivity patterns of one participant can do better at predicting that participant's functional activation than another participant's connectivity patterns. Unlike any of the analyses above, this relied on identifying the same voxel spatially across participants, so each participant in Group 2 was registered to MNI space, and subsequently onto each other participant's native anatomical space. Functional predictions for each participant were then made based on each other participant's connectivity pattern. A participant's own connectivity values were better at predicting their own functional activation than other participants' connectivity values ($T(419) = 11.67$, paired t-test, $P = 0$). Thus, the connectivity model is picking up on relationships between functional responses and connectivity patterns that capture individual variation.

Discussion

The present study provides evidence of a direct relationship between structural connectivity and function in the human brain. Specifically, we demonstrate that the responses to faces within an individual's right fusiform gyrus can be predicted from that individual's patterns of structural connectivity alone. This approach further reveals which targets are most influential in predicting function. Voxels with higher responses to faces had characteristic patterns of connectivity to other brain regions that distinguished them from neighboring voxels with lower responses to faces, or higher responses to scenes.

The connectivity model outperformed the random permutation control, indicating that there exists a strong relationship between connectivity and function. Moreover, it outperformed the distance control, suggesting that spatial information alone is insufficient for predicting functional activity and that connectivity offers information above and beyond the topographic information inherently embedded within it (due to the posited small-world organization of cortical connectivity[24,25]). The relationship between function and spatial information was highly variable across participants, while the connectivity data was consistent across participants in its relationship with the functional responses. When compared to the group-average benchmark, a standard method of defining face-selective ROIs in fMRI studies, connectivity was a significantly better predictor of the individual's actual activation pattern in over seventy-percent of the participants. One reason that the group-average did not successfully predict the activation pattern could be due to the high variability of activation loci, relative to the standard template (e.g.[26]).

While we have treated spatial metrics as potential confounds and controlled for them by using distance and group activation models as controls, future studies may build other geometric

models which do predict inter-subject variability in functional activation. For example, detailed models of cortical folding patterns[27], myelination[28], and/or cortical thickness[29] may be detectable with MRI and predictive of functional regions. Connectivity can provide a complementary source of evidence in some cases, whereas in others it may be the only gross morphological marker available.

Despite spatial variability in functional responses, the connectivity model was highly accurate across participants. We found that the spatial distribution of face- and scene-selectivity varies in tandem with connection strength to their most predictive targets. A direct analysis of subject-to-subject variability revealed that while each participant's connectivity profile does well at predicting their own functional response, it predicts another participant's functional responses relatively poorly. Overall, the connectivity patterns appeared highly sensitive to individual variation in function.

While the results from Group 1 are striking, they could be specific to one dataset[22]. The findings from Group 2 demonstrate that this is not the case: the connectivity model's predictions from Group 1 were much more accurate than both the distance and group-average models in over seventy percent of the new group of participants. This result was especially remarkable, because the participants in Group 2 had been scanned while performing a different functional task. The two tasks differed in the type of stimuli presented (1s static images versus 3s movie-clips), type of design (event-related versus block), number of runs (1 versus 3), and scan parameters (also see **Methods** for other differences). Further, the structural connectivity measures in this second group were acquired using a DWI sequence with half as many gradient directions (30 versus 60), indicating the generalizability of the connectivity model across functional tasks and diffusion sequences.

This analysis also reveals the target brain regions for which connectivity with the fusiform is most predictive of face- or scene-selective activity in the fusiform. Face-selective fusiform voxels were predicted by connectivity with regions that have been previously reported to have a role in face processing, such as the inferior and superior temporal cortices (e.g.[30, 31]). Scene-selective voxels, on the other hand, were best predicted by their connectivity to key brain areas involved with scene recognition, such as the isthmuscingulate (containing the retrosplenial cortex) and the parahippocampal cortex[10, 32, 33]. Unlike functional connectivity, structural connectivity models are naïve to the functional responses of the target regions. Therefore, a region need not be category selective to be connected (and predictive of) selective voxels in the fusiform. For example, unexpected predictors of face selectivity were also discovered, such as the cerebellar cortices. Even though the cerebellum is not commonly considered as part of the "core" or "extended" face processing network[3, 30, 34], tracer[35-37] studies have revealed disynaptic connections with extrastriate visual cortices via pons, which tractography is able to reconstruct (see **Supplementary Fig. 1**,**2**), and is corroborated by functional connectivity[38]. Future studies may explore these relationships to further expand on the role of functional responses in components of a structural network. Novel structure-function relationships could be investigated in macaques with functional and connectivity data, and subsequently validated more directly through more invasive techniques involving tracer injections (e.g.[39 ,40]).

The final connectivity model also provides a framework with which to evaluate the impact of the most predictive targets and their spatial distribution. The model built from only the significantly predictive targets resulted in more accurate predictions than the predictions based on all of the target regions. While some of the best predictors from this model were nearby regions, most of them were distant to the fusiform; additional analyses excluding the fusiform's

neighbors (**Supplementary Materials**) revealed that while proximal targets are part of the fusiform's network, they do not fully account for the connectivity model's performance. Altogether, a distributed network of brain regions characterizes category-specific visual processing in the fusiform gyrus.

The connectivity fingerprint has practical applications, both for defining ROIs independently of a task, and also for exploring group differences in structural connectivity signatures. Researchers or clinicians can apply the relationships discovered here to predict functional activation at the single-subject level in populations who do not or cannot have a functional localizer, and should expect that this will be a more accurate prediction than group-based methods. The connectivity model provided here can also be directly compared to a connectivity model built from specific patient populations. For instance, compromised structural connectivity in congenital prosopagnosics has previously been suggested to play a role in their deficits of face-recognition, in light of their surprisingly normal functional activation in the fusiform[41]. This type of analysis can shed light on which components (if any) of the fusiform connectional fingerprint are altered or compromised in individuals with congenital prosopagnosia. A similar analysis can be used to explore possible substrates of face-processing differences in autism, normal development, and aging.

Future studies can also extend the present methods to other brain regions and contrasts that are commonly used as functional localizers, such as retinotopy in visual cortices, scene-selectivity in the parahippocampal place area[10], or expression-specificity in the superior temporal sulcus. In some cases, more complex or nonlinear approaches might better capture the relationship of connectivity and function. We implemented a linear fit in order to provide more parsimonious interpretations and to establish the feasibility of modeling structure-function

relationships. Since these relationships are probably not strictly linear in a complex system such as the brain (**Supplementary Fig. 3**), future work can expand these findings, creating better models, and elucidating a more detailed relationship between connectivity and function. Additionally, voxel-to-voxel tractography may help to more finely characterize the structure-function relationships identified here.

These findings open a window into the coupling between structural and functional organization in the brain. The operations of a brain region are determined by both its intrinsic properties (i.e., cytoarchitecture) that likely determine the operations that it can perform, and the extrinsic connectivity that defines the input/output relations of that brain region. Neuroimaging can relate localized functions (via fMRI) to input/output patterns of cortical connectivity (via probabilistic tractography) in an individual. The present findings demonstrate that brain structure/function relations can be defined for category-selective functional activation.

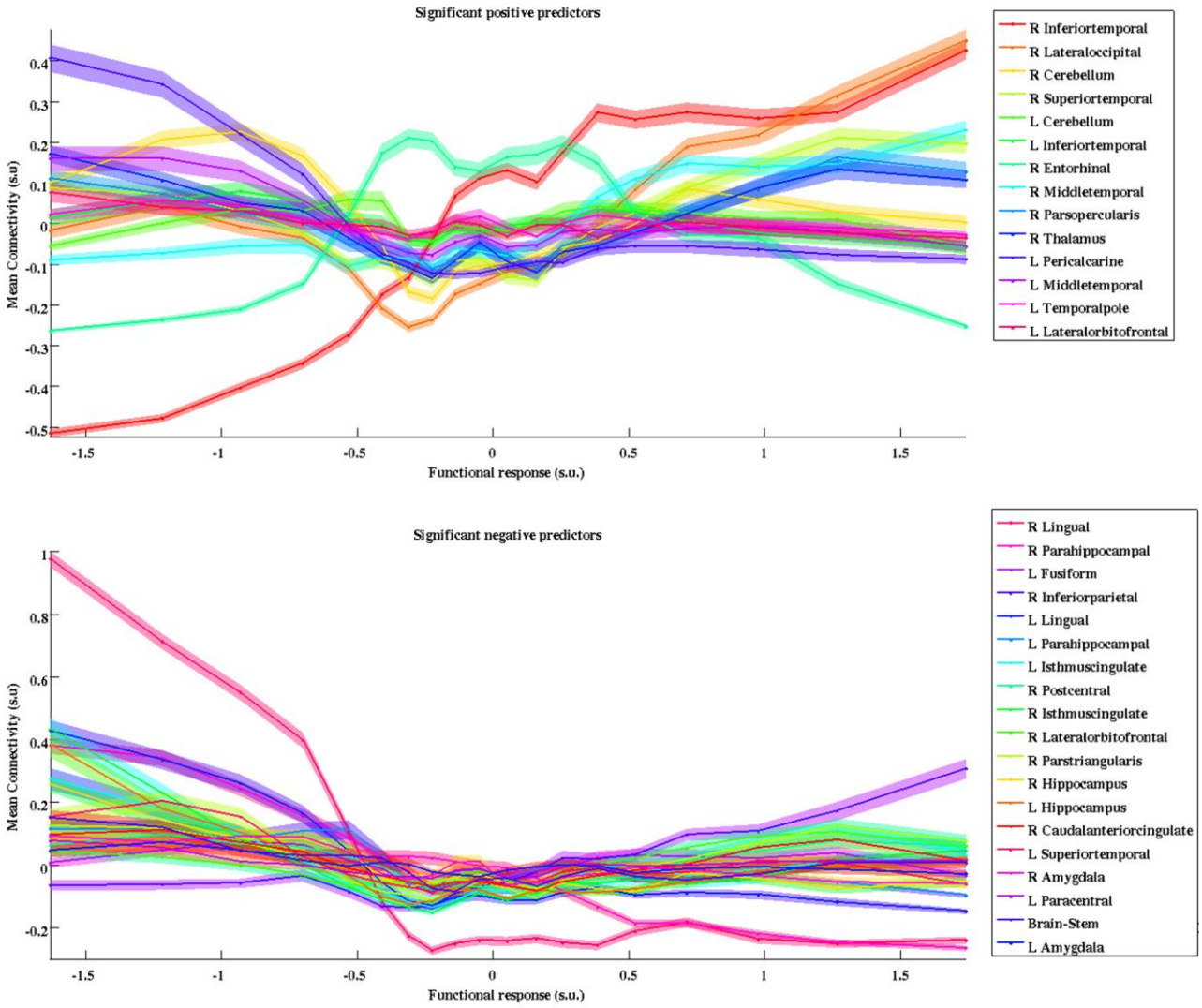

Supplementary Figure 3. Relationship between connectivity and selectivity.

Mean connectivity weights for the significantly predictive targets (**a** positive, **b** negative) are plotted for groups of voxels binned by their functional selectivity, sliding across each fifth percentile. Shaded regions represent standard error.

Supplementary Results and Discussion

Initial parametric tests

An initial analysis was performed to determine whether there were connectivity differences between the most face- and scene-selective voxels in the fusiform. We categorized voxels as highly face or scene selective if they responded at least two standard deviations above or below the mean, respectively, in the contrast of faces > scenes. A random effects ANOVA comparing positive and negative voxels (with participants treated as random effects) was performed per target region. Among the 85 target regions, 34 of them were significantly different between face-selective and scene-selective voxels in their fusiform connectivity, at $P < 0.05$, Bonferroni corrected (**Supplementary Table 1**). This initial finding suggested that the data possessed sufficient structure for its use in prediction. All further analyses were performed on all voxels and targets (regardless of their significance in these initial tests), treating both connectivity and functional activation as continuous variables.

Regression models excluding neighboring regions (Group 1 & 2)

As a further test of the influence of immediate spatial influence on the connectivity analysis, we included additional control models for connectivity and distance by excluding the regions neighboring the right fusiform, and compared their prediction errors. A regression model was built on Group 1 using LOOCV procedure, and tested on Group 2, as described in **Methods**. This time, however, connectivity patterns to the five regions immediately neighboring the right fusiform were excluded from the regression model. Distance models were also constructed in a similar fashion, but by training a model to predict T-values of fusiform voxels based on Euclidian distance to each target region, rather than connection probability to each

target. For this analysis, distances to the neighboring cortices were also excluded from the model. As before, the model was built from Group 1 using LOOCV, and tested on Group 2. MAE and AE were calculated as described in **Methods**, and were used to compare average and absolute prediction errors between the models with paired t-tests.

Connectivity models in the cross-validation group predicted actual fusiform activation with an MAE of 0.73 ± 0.008; this was higher than the previous model's MAE which did include connectivity to all the neighboring regions ($T(22) = 8.36$, $P = 2.81\times10^{-8}$). However, as was true for the original connectivity model, MAE comparisons between these control connectivity models and corresponding distance models (also built by excluding the neighbors) revealed better performance by connectivity ($T(22) = -3.73$, $P = 1.17\times10^{-3}$). The group-average model, which was identical to the model described in **Methods**, since it was constructed from whole-brain contrast maps using typical analysis methods, did not perform any better than the new connectivity models ($T(22) = 1.58$, $P = 0.13$).

We applied the connectivity model (excluding the neighbors) derived from all the subjects from Group 1, to the connectivity data of subjects in Group 2. While the MAEs of this new model (0.75 ± 0.009) were higher than those of the previous connectivity model ($T(20) = 4.37$, $P = 2.97\times10^{-4}$), they still outperformed the corresponding distance models by MAE ($T(20) = -8.17$, $P = 8.43\times10^{-8}$). Further, these MAEs were better than the previous group-average model, although this did not reach significance (group MAE = 0.82 ± 0.039; $T(20) = -2.01$, $P = 0.06$).

Regression models on the left fusiform gyrus

We replicated our main analyses for models of connectivity, distance, and group-average, in exactly the same manner but on the left fusiform gyrus. Comparisons of prediction errors between right and left fusiform models were performed by two-tailed t-tests (due to an unequal number of voxels in native-space left & right fusiform) while comparisons of models within the left fusiform were subject to paired t-tests as before. In Group 1, connectivity models of the left fusiform predicted the left fusiform's actual activation with an MAE of 0.67 ± 0.02; this was not worse than the prediction errors of the right fusiform models ($T(22) = 1.14$, $P = 0.27$). Just as was reported for the right fusiform, the MAE comparisons between the left fusiform's connectivity models and their corresponding distance models (MAE = 1.07 ± 0.105) revealed better performance by connectivity ($T(22) = -3.78$, $P = 1.03\times10^{-3}$). The group-average model was built identically to the procedure described in **Methods**, but the values were extracted from the left, not right fusiform. This model performed worse (MAE = 0.74 ± 0.034) than the left fusiform's connectivity model at near significance ($T(22) = 2$, $P = 0.057$).

We applied the final connectivity model for the left fusiform from Group 1 to the left fusiform connectivity data of subjects in Group 2. The MAEs of this new model (0.69 ± 0.02) were no different than those of the right fusiform connectivity model ($T(20) = 0.74$, $P = 0.47$). The left fusiform connectivity models outperformed the corresponding distance models (MAE = 0.73 ± 0.006; $T(20) = -3.09$, $P = 5.80\times10^{-3}$). Further, these MAEs were better than the corresponding group-average model (MAE = 0.82 ± 0.039; $T(20) = -3.86$, $P = 9.28\times10^{-4}$). Given previous research on the differences between the right and left fusiform's functional selectivity profiles (for faces and words respectively), a future extension of this study would be

to examine the specificity of connectivity-based models in predicting those selective responses and compare their predictive networks.

References:

1. Johansen-Berg, H., *et al.* Changes in connectivity profiles define functionally distinct regions in human medial frontal cortex. *Proceedings of the National Academy of Sciences of the United States of America* **101**, 13335 (2004).

2. Passingham, R.E., Stephan, K.E. & Kotter, R. The anatomical basis of functional localization in the cortex. *Nat Rev Neurosci* **3**, 606-616 (2002).

3. Haxby, J.V., *et al.* The effect of face inversion on activity in human neural systems for face and object perception. *Neuron* **22**, 189-199 (1999).

4. Tsao, D.Y., Schweers, N., Moeller, S. & Freiwald, W.A. Patches of face-selective cortex in the macaque frontal lobe. *Nat Neurosci* **11**, 877-879 (2008).

5. Perrett, D.I., Hietanen, J.K., Oram, M.W. & Benson, P.J. Organization and functions of cells responsive to faces in the temporal cortex. *Philos Trans R Soc Lond B Biol Sci* **335**, 23-30 (1992).

6. Tsao, D.Y., Freiwald, W.A., Tootell, R.B. & Livingstone, M.S. A cortical region consisting entirely of face-selective cells. *Science* **311**, 670-674 (2006).

7. Moeller, S., Freiwald, W.A. & Tsao, D.Y. Patches with links: a unified system for processing faces in the macaque temporal lobe. *Science* **320**, 1355-1359 (2008).

8. Kanwisher, N., McDermott, J. & Chun, M.M. The fusiform face area: a module in human extrastriate cortex specialized for face perception. *J Neurosci* **17**, 4302-4311 (1997).

9. Kanwisher, N., Stanley, D. & Harris, A. The fusiform face area is selective for faces not animals. *Neuroreport* **10**, 183-187 (1999).

10. Epstein, R. & Kanwisher, N. A cortical representation of the local visual environment. *Nature* **392**, 598-601 (1998).

11. Barton, J.J., Press, D.Z., Keenan, J.P. & O'Connor, M. Lesions of the fusiform face area impair perception of facial configuration in prosopagnosia. *Neurology* **58**, 71-78 (2002).

12. Pitcher, D., Walsh, V., Yovel, G. & Duchaine, B. TMS evidence for the involvement of the right occipital face area in early face processing. *Curr Biol* **17**, 1568-1573 (2007).

13. McNeil, J.E. & Warrington, E.K. Prosopagnosia: a face-specific disorder. *Q J Exp Psychol A* **46**, 1-10 (1993).

14. Landis, T., Cummings, J.L., Christen, L., Bogen, J.E. & Imhof, H.G. Are unilateral right posterior cerebral lesions sufficient to cause prosopagnosia? Clinical and radiological findings in six additional patients. *Cortex* **22**, 243-252 (1986).

15. McCarthy, G., Puce, A., Gore, J.C. & Allison, T. Face-specific processing in the human fusiform gyrus. *Journal of Cognitive Neuroscience* **9**, 605-610 (1997).

16. Behrens, T.E., *et al.* Non-invasive mapping of connections between human thalamus and cortex using diffusion imaging. *Nat Neurosci* **6**, 750-757 (2003).

17. Behrens, T.E., *et al.* Characterization and propagation of uncertainty in diffusion-weighted MR imaging. *Magn Reson Med* **50**, 1077-1088 (2003).

18. Catani, M., Jones, D.K., Donato, R. & Ffytche, D.H. Occipito-temporal connections in the human brain. *Brain* **126**, 2093-2107 (2003).

19. Seltzer, B. & Pandya, D.N. Parietal, temporal, and occipital projections to cortex of the superior temporal sulcus in the rhesus monkey: a retrograde tracer study. *J Comp Neurol* **343**, 445-463 (1994).

20. Gloor, P. *The Temporal Lobe and Limbic System* (Oxford University Press, Inc., New York, New York, 1997).

21. Gholipour, A., Kehtarnavaz, N., Briggs, R., Devous, M. & Gopinath, K. Brain functional localization: a survey of image registration techniques. *IEEE Trans Med Imaging* **26**, 427-451 (2007).

22. Hastie, T., Tibshirani, R. & Friedman, J.H. *The elements of statistical learning : data mining, inference, and prediction* (Springer, New York, 2009).

23. Golland, P. & Fischl, B. Permutation tests for classification: towards statistical significance in image-based studies. *Inf Process Med Imaging* **18**, 330-341 (2003).

24. Hilgetag, C.C. & Kaiser, M. Clustered organization of cortical connectivity. *Neuroinformatics* **2**, 353-360 (2004).

25. Sporns, O. & Zwi, J.D. The small world of the cerebral cortex. *Neuroinformatics* **2**, 145-162 (2004).

26. Saxe, R., Moran, J.M., Scholz, J. & Gabrieli, J. Overlapping and non-overlapping brain regions for theory of mind and self reflection in individual subjects. *Soc Cogn Affect Neurosci* **1**, 229-234 (2006).

27. Hinds, O.P., *et al.* Accurate prediction of V1 location from cortical folds in a surface coordinate system. *Neuroimage* **39**, 1585-1599 (2008).

28. Annese, J., Gazzaniga, M. & Toga, A. Localization of the human cortical visual area MT based on computer aided histological analysis. *Cerebral Cortex* **15**, 1044 (2005).

29. Dickerson, B., *et al.* Detection of cortical thickness correlates of cognitive performance: reliability across MRI scan sessions, scanners, and field strengths. *Neuroimage* **39**, 10-18 (2008).

30. Ishai, A. Let's face it: it's a cortical network. *Neuroimage* **40**, 415-419 (2008).

31. Kanwisher, N. & Yovel, G. The fusiform face area: a cortical region specialized for the perception of faces. *Philos Trans R Soc Lond B Biol Sci* **361**, 2109-2128 (2006).

32. Epstein, R.A. Parahippocampal and retrosplenial contributions to human spatial navigation. *Trends Cogn Sci* **12**, 388-396 (2008).

33. Sewards, T.V. Neural structures and mechanisms involved in scene recognition: a review and interpretation. *Neuropsychologia* **49**, 277-298 (2011).

34. Haxby, J.V., Hoffman, E.A. & Gobbini, M.I. The distributed human neural system for face perception. *Trends Cogn Sci* **4**, 223-233 (2000).

35. Schmahmann, J.D. & Pandya, D.N. Course of the fiber pathways to pons from parasensory association areas in the rhesus monkey. *J Comp Neurol* **326**, 159-179 (1992).

36. Schmahmann, J.D. & Pandya, D.N. Prelunate, occipitotemporal, and parahippocampal projections to the basis pontis in rhesus monkey. *J Comp Neurol* **337**, 94-112 (1993).

37. Glickstein, M., *et al.* Visual pontocerebellar projections in the macaque. *J Comp Neurol* **349**, 51-72 (1994).

38. O'Reilly, J.X., Beckmann, C.F., Tomassini, V., Ramnani, N. & Johansen-Berg, H. Distinct and overlapping functional zones in the cerebellum defined by resting state functional connectivity. *Cereb Cortex* **20**, 953-965 (2009).

39. Dauguet, J., *et al.* Comparison of fiber tracts derived from in-vivo DTI tractography with 3D histological neural tract tracer reconstruction on a macaque brain. *Neuroimage* **37**, 530-538 (2007).

40. Peled, S., Berezovskii, V., Hendrickson, P., Born, R. & Westin, C. Histological validation of DTI using WGA-HRP in a macaque. 1323 (2005).

41. Thomas, C., *et al.* Reduced structural connectivity in ventral visual cortex in congenital prosopagnosia. *Nat Neurosci* **12**, 29-31 (2009).

42. Reese, T.G., Heid, O., Weisskoff, R.M. & Wedeen, V.J. Reduction of eddy-current-induced distortion in diffusion MRI using a twice-refocused spin echo. *Magn Reson Med* **49**, 177-182 (2003).

43. IASLab. Development of the Interdisciplinary Affective Science Laboratory (IASLab) Face Set was supported by the National Institutes of Health Director's Pioneer Award (DP1OD003312) to Lisa Feldman Barrett. Available on-line at www.affective-science.org.

44. Oliva, A. & Torralba, A. Modeling the Shape of the Scene: A Holistic Representation of the Spatial Envelope. *International Journal of Computer Vision* **42**, 145-175 (2001).

45. Dale, A.M. Optimal experimental design for event-related fMRI. *Hum Brain Mapp* **8**, 109-114 (1999).

46. Pitcher, D., Dilks, D.D., Saxe, R.R., Triantafyllou, C. & Kanwisher, N. Differential selectivity for dynamic versus static information in face-selective cortical regions. *Neuroimage* (2011).

47. Fischl, B., *et al.* Automatically parcellating the human cerebral cortex. *Cereb Cortex* **14**, 11-22 (2004).

48. Fischl, B., *et al.* Whole brain segmentation: automated labeling of neuroanatomical structures in the human brain. *Neuron* **33**, 341-355 (2002).

49. Desikan, R.S., *et al.* An automated labeling system for subdividing the human cerebral cortex on MRI scans into gyral based regions of interest. *Neuroimage* **31**, 968-980 (2006).

50. Behrens, T.E., Berg, H.J., Jbabdi, S., Rushworth, M.F. & Woolrich, M.W. Probabilistic diffusion tractography with multiple fibre orientations: What can we gain? *Neuroimage* **34**, 144-155 (2007).

Chapter 3

Anatomical connectivity predicts whole-brain functional responses to visual categories.

Work in collaboration with:

Saygin Z.M., Koldewyn K., Saxe, R.R., Gabrieli J.D.E., Kanwisher N.

Structural connectivity is among the most important constraints on a network since it restricts and defines the sort of information that can be processed. The functional responses of a voxel should therefore be strongly influenced by its pattern of connectivity; correspondingly, patterns of connectivity should be highly predictive of function. We present the use of anatomical connectivity to predict functional activity in each gray matter voxel of the brain. Diffusion-weighted images and fMRI images were acquired from two groups of healthy subjects. Probabilistic diffusion tractography was performed from each anatomically-defined parcel to all other anatomical parcels. For each parcel, we modeled the fMRI data as a function of connection probability using linear regressions. The models surpassed performance distributions generated from randomly permuted data, indicating that the connectivity data are structured sufficiently for prediction. The models also accurately predicted fMRI activation in new participants in (two different groups) using only their DWI data. Further, connectivity-based predictions also outperformed a group-average benchmark model, both across the whole brain and within each functionally-specific region of interest (fROI), in the two groups of participants. Overall, we

found that connectivity patterns account for individual variability and are unique for different functions. These results support the hypothesis that connectivity is predictive of functional specialization at a voxel-wise grain across the cortex, thus confirming and extending a fundamental assumption in neuroscience.

Introduction

A deep-rooted assumption in neuroscience holds that a region's functional capabilities are primarily determined by its physical structure. In other words, there should exist a causal relationship between the brain's anatomical features and its functional responses, which should lead towards explanatory, rather than descriptive accounts of brain function. Among these anatomical features, connectivity is especially important since it sculpts a network's computational landscape. Thus, it should strongly influence a voxel's functional responses, and likewise, a voxel's connectivity pattern should be highly predictive of function.

By measuring both structural connectivity and neural responses in the same individual, recent neuroimaging studies have shown that changes in DWI connectivity occur at the boundaries of low-level functionally defined regions (e.g. Johansenberg et al. 2004 for supplementary motor area, or SMA and pre-SMA). However, it is unknown whether connectivity patterns can also define the boundaries for higher-level regions or those that cannot yet be identified via anatomy/cytoarchitectonics and are highly variable across individuals (e.g. Frost & Goebel 2012; Saxe, Brett, & Kanwisher 2006).

We have developed a new method of testing the hypothesis that structural connectivity determines functional specificity, and previously tested this method in the fusiform gyrus (Saygin, Osher et al. 2012). Specifically, it was shown that the face selectivity of each voxel in the fusiform could be predicted from the strength of connection of that voxel to each of 85 anatomically defined regions of the rest of the brain (its unique connectivity profile, or fingerprint, CF), as measured through DWI (**Figure 1**). The fMRI response of each fusiform voxel to faces > scenes (red to blue circles) was paired with that voxel's 85-dimensional CF vector (rows of grayscale circles). The fMRI - CF pairings were concatenated across all fusiform

voxels and all subjects, and a linear regression was trained to learn the systematic relationship (f(x) Fig.1) between fMRI responses and CFs. This relationship was then applied to each fusiform voxel's CF in a new subject, resulting in a predicted fMRI value for each voxel (**Figure 1**).

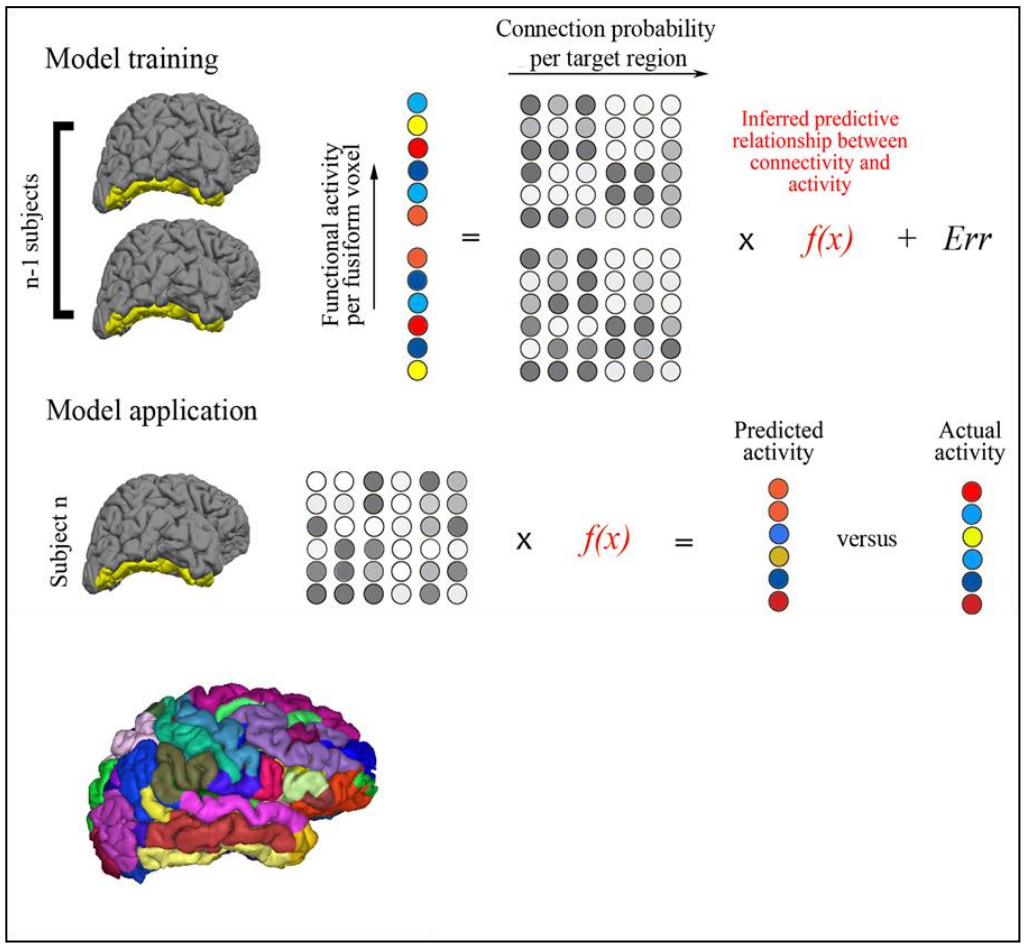

Figure 1: Overall methodology of predicting fMRI responses from DWI connectivity.

a. Reprint from Saygin, Osher et al. 2012. Face selectivity of each voxel in the fusiform is predicted from the strength of connection of that voxel to each of 85 anatomically defined regions of the rest of the brain (its unique CF), as measured through DWI. The fMRI response of each fusiform voxel to faces > scenes (red to blue circles) was paired with that voxel's 85-

dimensional CF vector (rows of grayscale circles). The fMRI - CF pairings were concatenated across all fusiform voxels and all subjects, and a linear regression was trained to learn the systematic relationship (*f(x)*) between fMRI responses and CFs. This relationship was then applied to each fusiform voxel's CF in a new subject, resulting in a predicted fMRI value for each voxel. **b.** The fusiform methodology was performed separately for each anatomically parcel, then combined and interpolated to produce predicted fMRI value for each gray matter voxel of the brain.

However, these connectivity-based predictions of fMRI activation were restricted to face responses, and only in the fusiform gyrus. We now extend this method to the whole brain (and other visual categories that evoke robust fMRI responses) to ask: are connectivity patterns predictive of fMRI responses during visual categorical perception of faces, bodies, objects, and scenes?

Previous studies in macaques would suggest that the extrinsic connectivity pattern of each visual cortical region is indeed unique and perhaps predictive of each region's broad role within the visual-processing hierarchies (e.g. Ungerleider & Mishkin 1982; Felleman & Van Essen 1991). However, there is great functional diversity within these cortical regions, whereby different neural clusters within an area preferentially respond to different categories or object features (e.g. Tsao et al. 2006; Colby & Goldberg 1999; Kanwisher & Dilks, in press). The relationship between this fine-grained pattern of functional responses and extrinsic connections remains unknown. By testing fMRI responses to a variety of functional domains, we will ascertain whether the relationship between connectivity and function is generally true across the cortex and across diverse visual domains.

Methods

Participants.

The study included 28 participants (mean age=25.6, 12M:16F) who were recruited from the greater Boston area. Participants were screened for history of mental illness, gave written informed consent, and were compensated at $30 per hour. The study was approved by the Massachusetts Institute of Technology and Massachusetts General Hospital ethics committees.

DWI acquisition parameters and tractography.

DWI data were acquired using echo planar imaging (64 slices, voxel size 2 × 2 × 2 mm, 128 × 128 base resolution, diffusion weighting isotropically distributed along 30 directions, *b*-value 700 s mm^{-2}) on a 3-T Siemens scanner with a 32-channel head-coil (Reese et al. 2003). A high resolution (1 mm^3) three-dimensional magnetization-prepared rapid acquisition with gradient echo (MPRAGE) scan was acquired on these participants.

Automated cortical and subcortical parcellation was performed in each participant's T1 scan, using the Destrieux atlas (Desikan et al. 2006) from Freesurfer 5.1 (Fischl et al. 2002, 2004) to define 167 cortical and subcortical regions. Automated segmentation results were reviewed for quality control and were then registered to each individual's diffusion images and used as the seed and target regions for fiber tracking. The resulting cortical and subcortical targets were then checked and corrected for automatic parcellation or segmentation errors if necessary. The principal diffusion directions were calculated per voxel, and probabilistic diffusion tractography was carried out using FSL-FDT (Behrens et al. 2007) with 5,000 streamline samples in each seed voxel to create a connectivity distribution to each of the target regions, while avoiding a mask consisting of the ventricles. Each of the 167 regions was used as a seed region and tractography was carried out to all 166 remaining regions, or targets. Thus,

every voxel within each parcel is described by a vector of connection probabilities to each other brain region.

fMRI acquisition parameters and analysis.

Stimuli for the fMRI consisted of 3-s movie clips of faces, bodies, scenes, objects and scrambled objects. Movies of faces and bodies were filmed against a black background and framed to reveal just the faces or bodies of seven individuals, shown one at a time. Scenes consisted primarily of pastoral scenes filmed through a car window while driving slowly through the countryside or suburb. Objects were selected specifically to minimize any suggestion of animacy of the object itself or of an invisible actor pushing the object. Scrambled object clips were constructed by dividing each object movie clip into a 15 × 15 box grid and spatially rearranging the location of each of the resulting boxes. Pilot testing indicated that a contrast of the response for moving faces versus moving objects identified the same FFA as that identified in a standard static localizer. Further studies show that the FFA responds similarly to movies of faces as to static snapshots of faces (Pitcher et al. 2011).

Functional data were acquired over four block-design functional runs (gradient echo sequence 2,000 ms TR, 30 ms TE, 90° flip, 234 volumes, 3 × 3 × 3 mm voxel size). Each functional run contained three 18-s fixation blocks at the beginning, middle and end of the run. During these blocks, a series of six uniform color fields were presented for 3 s each. Each run also contained two sets of five consecutive stimulus blocks (faces, bodies, scenes, objects or scrambled objects) sandwiched between these rest blocks, resulting in two blocks per stimulus category per run. Each block lasted 18 s and contained six 3-s movies clips from each of the five stimulus categories. The order of stimulus category blocks in each run was palindromic, and

specific movie clips were chosen randomly to be presented during the block. Participants were asked to passively view the stimuli.

Functional data were analyzed with FSL software (http://www.fmrib.ox.ac.uk/fsl/). Images were motion corrected, smoothed (5 mm Gaussian kernel, full width at half maximum) and detrended, and were fit using a standard gamma function ($\delta = 2.25$ and $\tau = 1.25$). Data were not spatially normalized. Statistical modeling was then performed using a general linear model on the preprocessed functional images. Next, *t*-maps corresponding to each contrast of interest were overlaid on each participant's high-resolution anatomical image. The contrasts were as follows: Faces > Objects, Bodies > Objects, Scenes > Objects, Objects > Scrambled objects.

Each participant's functional image for each contrast was registered to his or her diffusion-weighted image. Because we were interested in predicting relative activation values that were independent of task-specific parameters such as the degrees of freedom, we standardized the *t*-statistic values across all gray matter parcels per participant. For each anatomical parcel, the mean functional value across the brain was subtracted from each voxel and divided by the standard deviation. The standardized value per voxel was then used for the subsequent regression models, which were built per region. Thus, every voxel is now also described by a vector of *t*-statistics for each functional contrast.

Regressions.

All analyses were performed on subject-specific anatomy, rather than extrapolation from a template brain, except for the group-average models. For the regression models, each observation was an individual voxel in native space, and there was no identifying or matching of

spatial location of voxels across participants. Further, the model was blind to the participant each voxel belonged to.

Subjects were divided into two groups (group 1 for leave-one-out cross-validation and group 2 for replication); this procedure ensures that any relationship learned from one set of data is separate from the data that is used to assess the accuracy of that learnt relationship.

Group 1: To predict function from connectivity, we used a leave-one-subject-out cross validation (LOOCV) routine, in which we excluded a single subject whose data we wish to predict, trained a model with all of the remaining subjects, and then applied the model to the left out subject. This routine was repeated for all subjects, generating independent predictions for all subjects. The model was designed as follows: every voxel of the modeled region has a neural response to a given functional contrast. Every voxel also has a vector of connection probabilities to each other brain region, illustrated in **Figure 1** across columns of the gray-scale circles. The predictive relationship between connectivity and neural activity was inferred via linear regression, resulting in a set of predictive coefficients. We then predicted the neural response for the left out subject, using only their connectivity data, and the model coefficients, resulting in a predicted value for every voxel of the modeled region.

In order to generate predictions for the entire brain, this procedure, from tractography to prediction, was repeated for every parcel, and concatenated. This was then compared to the participants' own observed fMRI images for that contrast, and absolute errors (AEs) were calculated (absolute value of actual – predicted per voxel). We also calculated the mean absolute error (MAE) and mean squared error (MSE) per anatomical parcel for each individual. Group 2: For each anatomical parcel, we generated a final linear regression model from all of the group 1 subjects' connectivity and fMRI data. We applied this final model of the relationship between

connectivity and function, to each group 2 subjects' connectivity data, to produce predicted fMRI maps per subject. Prediction accuracies were calculated by comparing these predictions to each participant's actual fMRI values (AE, MAE, and MSE were calculated in the same way as for group 1). The accuracies were tested against random permutations and other benchmarks (below). We also performed a one-way ANOVA on the mean absolute error across all gray matter voxels per subject for all of the functional contrasts to discover whether any contrasts were better predicted by connectivity than the others; post-hoc t-tests were used to identify the contrasts that were significantly better predicted than others (at $p < 0.05$ Bonferroni corrected for six pairwise comparisons).

Performance accuracy.

As a measure of accuracy, we measured the absolute error per voxel (reported in standardized units) per participant, by calculating the absolute difference between the predicted and actual values (AE, also see above). We used permutation tests to evaluate whether the connectivity-based prediction accuracies are significantly better than chance by using random permutation models (Golland & Fischl 2003). We shuffled the actual fMRI values and connection probability vectors, and permute across 5,000 of these random combinations. Thus each actual fMRI value was assigned to a different, randomly chosen, voxel's connection probability vector. This will generate a distribution of random prediction errors per participant and allow us to determine whether connectivity-based predictions are significantly more accurate than random noise generated from the same data (Bonferroni corrected at $p < .05$ for total number of comparisons). This gave us an empirical distribution of random MAE per participant which we can be used to assess the probability that the connectivity-based MAE is part of said distribution (see Saygin et al. 2012).

For each functional contrast, we produced a final connectivity model from all the subjects in group 1 and evaluated each anatomical parcel's model R^2. The R^2 is a standard metric of goodness-of-fit, and for these data, it reflects the proportion of the variance in fMRI activity across all of the voxels in the region and across all subjects that was accounted for by connectivity (the model is agnostic to which voxels belong to which subject; the voxels are merely concatenated across subjects per anatomical parcel). We separately correlated each parcel's R^2 with 2 metrics of functional selectivity: 1) the absolute value of the mean extremum across subjects, and 2) accuracy of multivoxel pattern analysis (MVPA; see Haxby et al. 2001), which reflect how well the response patterns across voxels within a parcel are able to differentiate between each functional condition.

Benchmark group-average models.

We also compared the prediction accuracies to a benchmark model to further test whether connectivity can predict function beyond what is possible beyond what can be predicted from a group analysis (see Saygin et al. 2012 for details). Group analyses are the current alternative for predicting functional activity based on other subjects' data. These were also made through LOOCV. Each participant's functional data were spatially normalized into MNI space with FSL and FreeSurfer, checked and corrected for registration errors, and superimposed to create composite maps. We performed a random-effects test on whole-brain fMRI data with SPM8 on each contrast image from all but one participant. The resulting *t*-statistic image, which was based on all the other participants in normalized space, was applied to the participant left out of the group analysis and was registered back into his or her native space. This resulted in a predicted value for each voxel. A final group-average t-statistic was also generated from all of the group 1 participants, and this group-average map was applied to each of the group 2 subjects to evaluate

group-based prediction accuracies of function. We performed a pair-wise *t*-test of mean absolute and squared prediction errors of all gray-matter voxels across the participants in groups 1 and 2 separately.

We then registered each subject's actual and predicted fMRI maps (based on the group-average and connectivity analyses separately) to a common Freesurfer CVS atlas (Postelnicu et al. 2009; Zollei et al. 2010). We also evaluated prediction accuracies in this space because it offers a common framework across participants (with minimum warping of anatomical data, Postelnicu et al. 2009; Zollei et al. 2010) and it is not the template we used for the group-average analysis, thus avoiding any potential confounds of using the same template space for accuracy evaluations. Further, probabilistic parcels of fROIs (based on a large independent sample of adults, Julian et al. 2012) were created in this CVS space, and we could therefore assess prediction accuracies for connectivity vs. group-average across the whole-brain, but also within each of these larger fROIs. We followed the procedure above for each of the four functional contrasts.

We performed a pair-wise *t*-test per participant across all gray-matter voxels within each of the fROI parcels. A criterion threshold of $P < 0.05/28$ (total number of subjects in group 1 and group 2) was used to report the number of participants whose activation pattern was better predicted by one model versus another.

To create binarized fROIs of the predicted and actual fMRI maps, we registered the probabilistic parcels of fROIs (Julian et al. 2012) from CVS space to each subject's diffusion images. For both the actual and predicted fMRI maps, we then binarized the top 10% of voxels within each of these parcels to create 7 face-specific fROIs, 3 object-specific, 6 scene-specific, and four object-specific regions (see **Table 1**). We used the modified Hausdorff distance (e.g.

Yendiki et al. 2011) to assess the accuracy of the predicted fROIs. We measured the distance from each point in the predicted fROI to the nearest voxel in the actual fROI and averaged across them to calculate the modified Hausdorff distance.

Results

For each region, we trained a linear regression on the voxel-wise fMRI and connection probabilities across subjects, applied the resulting model of the learned relationship between connectivity and function to a new participants' connectivity data, and calculated prediction accuracies by comparing these predictions to each participant's actual fMRI values (absolute error). We tested these accuracies against random permutation models (Section 1), evaluated the voxel-wise fMRI variance accounted for by the final connectivity models (Section 2), and compared the connectivity-based prediction accuracies to benchmark models (Section 3). We also compared predicted functional regions of interest (fROIs) to each individual's actual fROIs for each high-level visual domain (Section 4).

1. Connectivity-based predictions of functional contrasts closely match actual activation maps in individual subjects.

We evaluated the accuracy of the connectivity-based predictions of fMRI activity for each of the functional contrasts by comparing errors to random permutation models. For each subject, we calculated the prediction accuracies across all gray-matter voxels and in each cortical parcel separately. The contrast of Faces > Objects typically elicits activation in the posterior superior temporal sulcus, and in ventral temporal and occipital regions known as the fusiform face area (FFA) and occipital face area (OFA; **Table 1**).

Table 1. Functional domains and corresponding fMRI contrast and specialized brain regions (fROIs).

Function	Contrast	fROIs
face perception	faces > objects	fusiform face area, FFA
		occipital face area, OFA
		superior temporal sulcus, STS
		post. superior temporal sulcus, pcSTS
body perc.	bodies > objects	extrastriate body area, EBA
		fusiform body area, FBA
scene perc.	scenes > objects	parahippocampal place area, PPA
		transverse occipital sulcus, TOS
		retrosplenial cortex, RSC
object perc.	objects > scrambled	lateral occipital, LOC
		posterior fusiform sulcus, PFS

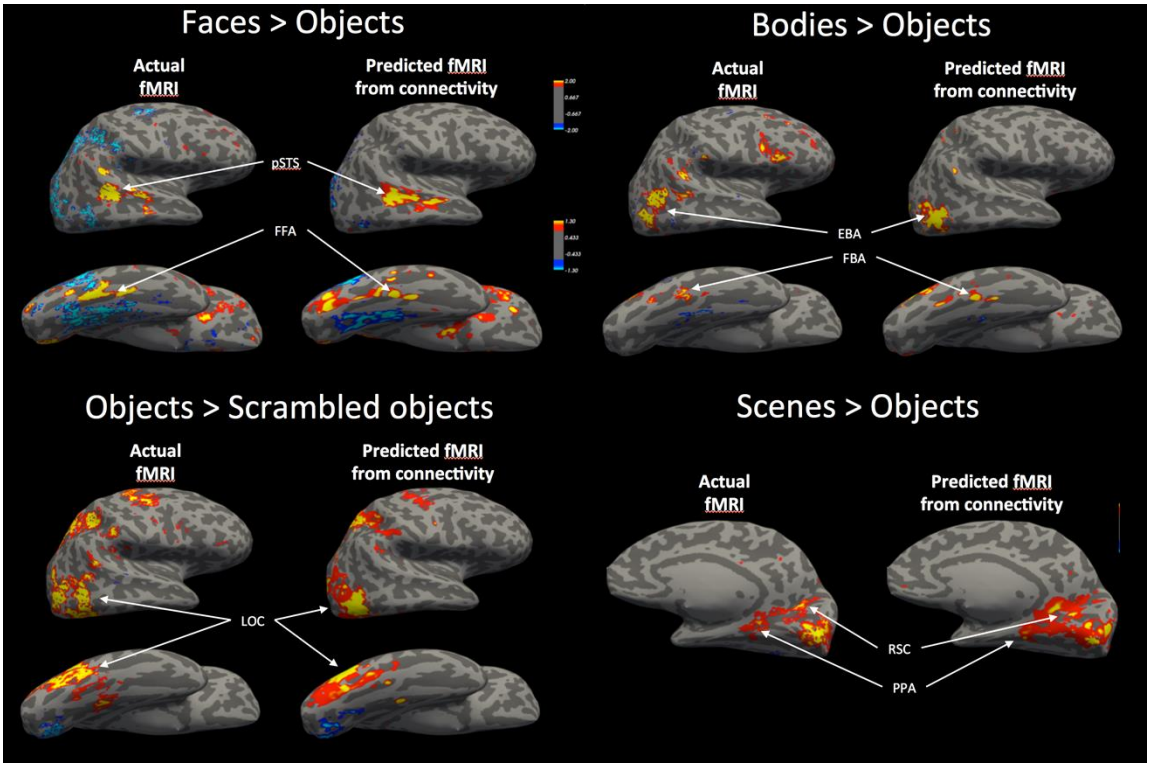

Figure 2: Visualization of prediction results on an example subject. Representative subject's actual and predicted activation images are up-sampled from the DWI structural image to the same participant's structural scan, and projected onto the participant's inflated brain surface. Predicted fMRI activation values (right column of each panel) for each visual category contrast closely match the actual fMRI values (left columns) for that contrast, especially in regions commonly identified as being functionally selective for that particular visual category (i.e. fROIs; see **Table 1**). (**a**) Faces > Objects (**b**) Bodies > Objects (**c**) Scenes > Objects (**d**) Objects > Scrambled Objects.

Figure 2a illustrates the results for a representative subject. The predicted response (**Figure 2a**), built solely from the same subject's connectivity data, is strikingly similar to the actual response. This qualitatively demonstrates how an individual's response pattern to Faces > Objects can be well predicted by that individual's connectivity pattern. The contrast of Bodies > Objects localizes the functionally defined regions known as the extrastriate body area (EBA) and the fusiform body area (FBA). Again, a subject's own connectivity patterns are capable of predicting these regions (**Figure 2b**). Scenes > Objects typically evokes activity along the ventral medial surface (Sewards et al. 2011). Some of the functional regions often associated with scene specificity are the parahippocampal place area (PPA) and retrosplenial cortex (RSC), and yet again we see that, a subject's connectivity pattern alone is highly predictive of their pattern of functional response (**Figure 2c**). Objects > Scrambled results in a distributed set of functional regions collectively known as the lateral occipital complex. Not only can connectivity capture this robust neural response, but it also accounts for the somewhat less characterized dorsal activity patterns, for example in the intraparietal sulcus (**Figure 2d**).

We calculated the absolute error (AE) per voxel as the difference between the predicted and actual fMRI images, and mean absolute error (MAE) as a measure of accuracy for each contrast (**Table 2**).

Table 2. Mean prediction errors and benchmark comparisons. Mean prediction errors (± standard error across participants) across all anatomical parcels for predicted fMRI activation to each functional contrast by connectivity models and group-average benchmarks. T-statistic and p-values are also reported for each contrast for the comparison of connectivity vs. group-average models. Negative t-values indicate lower prediction error (higher accuracy) for connectivity than group-average.

	Faces-Objects	**Bodies-Objects**	**Scenes-Objects**	**Objects-Scrambled**
MAE				
Group 1				
Connectivity	0.657±0.014	0.771±0.006	0.649±0.021	0.708±0.014
Group	0.775±0.019	0.977±0.012	0.764±0.028	0.847±0.025
Connectivity-Group *t*	-14.368	-26.488	-12.859	-10.118
Connectivity-Group *p*	6.12E-11	2.91E-15	3.47E-10	1.30E-08
Group 2				
Connectivity	0.680±0.017	0.784±0.009	0.662±0.019	0.718±0.020
Group	0.797±0.030	1.004±0.017	0.783±0.023	0.858±0.033
Connectivity-Group *t*	-6.687	-22.274	-7.915	-7.495
Connectivity-Group *p*	8.99E-05	3.51E-09	2.41E-05	3.71E-05
MSE				
Group 1				
Connectivity	0.789±0.025	1.005±0.010	0.769±0.048	0.877±0.028
Group	1.012±0.050	1.549±0.037	0.979±0.079	1.174±0.070
Connectivity-Group *t*	-8.172	-19.33	-6.357	-6.798
Connectivity-Group *p*	2.73E-07	5.22E-13	7.16E-06	3.11E-06
Group 2				
Connectivity	0.816±0.039	1.034±0.020	0.780±0.039	0.863±0.041
Group	1.062±0.085	1.644±0.056	1.025±0.065	1.180±0.091
Connectivity-Group *t*	-4.69	-16.071	-5.884	-5.669
Connectivity-Group *p*	1.14E-03	6.19E-08	2.34E-04	3.06E-04

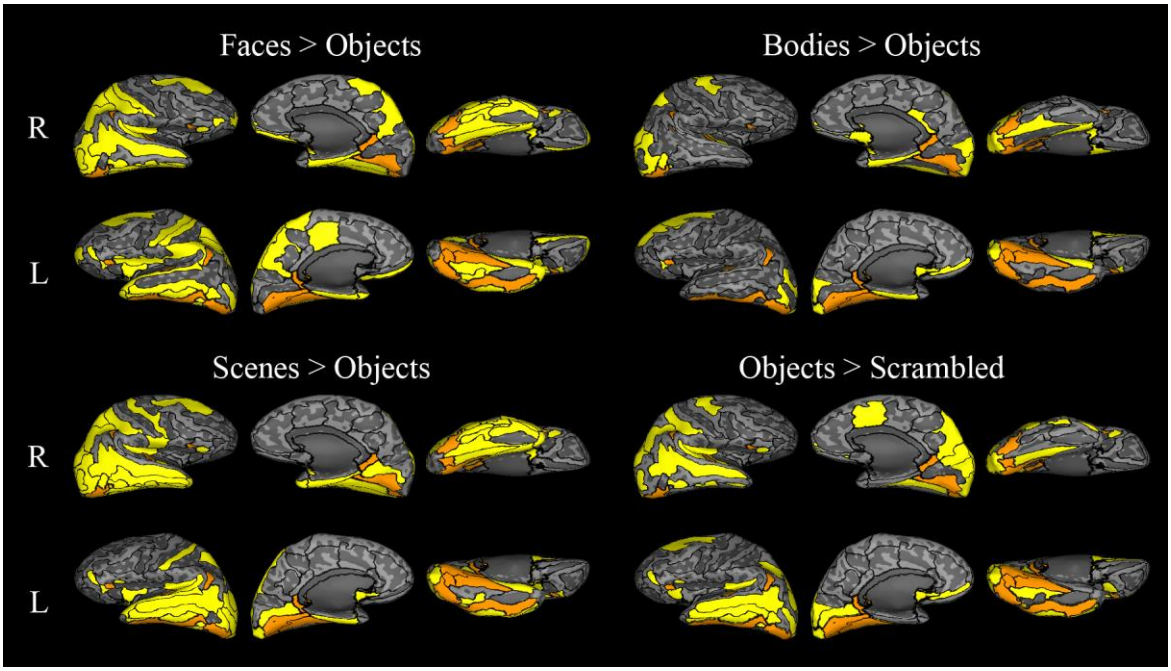

Figure 3. Prediction accuracies across cortical regions. For each perceptual category, cortical regions that passed random permutation testing in over 60% of subjects are colored yellow (projected on an inflated surface). Regions with connectivity patterns that accurately predict activation patterns equally well across all categories are labeled in orange.

We also performed random permutation tests[23] to statistically assess the performance of the connectivity model by generating a distribution of accuracies per subject from random models built from shuffled pairings between connectivity and functional responses. We identified the regions that passed permutation testing (at $p < 0.05$ Bonferroni corrected) in more than sixty percent of group 1 subjects. The regions whose connectivity patterns successfully predicted functional activity to each contrast were mainly ventral visual regions that are typically associated with each contrast (**Figure 3**). Certain regions had connectivity patterns that accurately predicted activation patterns equally well across all categories, such as right and left

inferior occipital gyri and sulci, while others were only accurate for a particular functional contrast (**Supplementary Table 1**).

Supplementary Table 1. List of cortical regions that accurately predicted activation patterns for all four functional contrasts in over sixty percent of subjects, and regions that were accurate only for one particular contrast. Note that this list does not include all the regions that were significant in each contrast, only those that were uniquely accurate for that contrast. G=gyrus, S=sulcus.

All contrasts	**Faces-Objects**	**Bodies-Objects**	**Scenes-Objects**	**Objects-Scrambled**
Left G and S occipital inf	Left G and S cingul Mid Post	Left S front middle	Left G temp sup Plan tempo	Left S circular insula ant
Left G cingul Post ventral	Left G and S frontomargin	Right G cingul Post dorsal	Right G and S subcentral	Right G and S cingul Mid Ant
Left G oc temp med Lingual	Left G and S paracentral	Right G subcallosal	Right G precentral	Right S parieto occipital
Left G temporal inf	Left G pariet inf Supramar		Right G temporal middle	
Left Lat Fis ant Horizont	Left G precuneus		Right Pole temporal	
Left S collat transv post	Left G rectus		Right S calcarine	
Left S interm prim Jensen	Left Pole temporal			
Left S oc temp med and Lingual	Left S central			
Left S temporal transverse	Left S circular insula sup			
Right G and S occipital inf	Right G and S frontomargin			
Right G cingul Post ventral	Right G and S paracentral			
Right G oc temp med Lingual	Right G postcentral			
Right Lat Fis ant Vertical	Right G rectus			
Right S collat transv post	Right S orbital lateral			
Right S interm prim Jensen				
Right S temporal transverse				

The number of subjects for which connectivity accurately predicted functional activation correlated positively with the response selectivity for that anatomical region (**Figure 4**). Regions with higher responses to the contrast, or greater selectivity for one visual category over another, were those regions that were better predicted by connectivity.

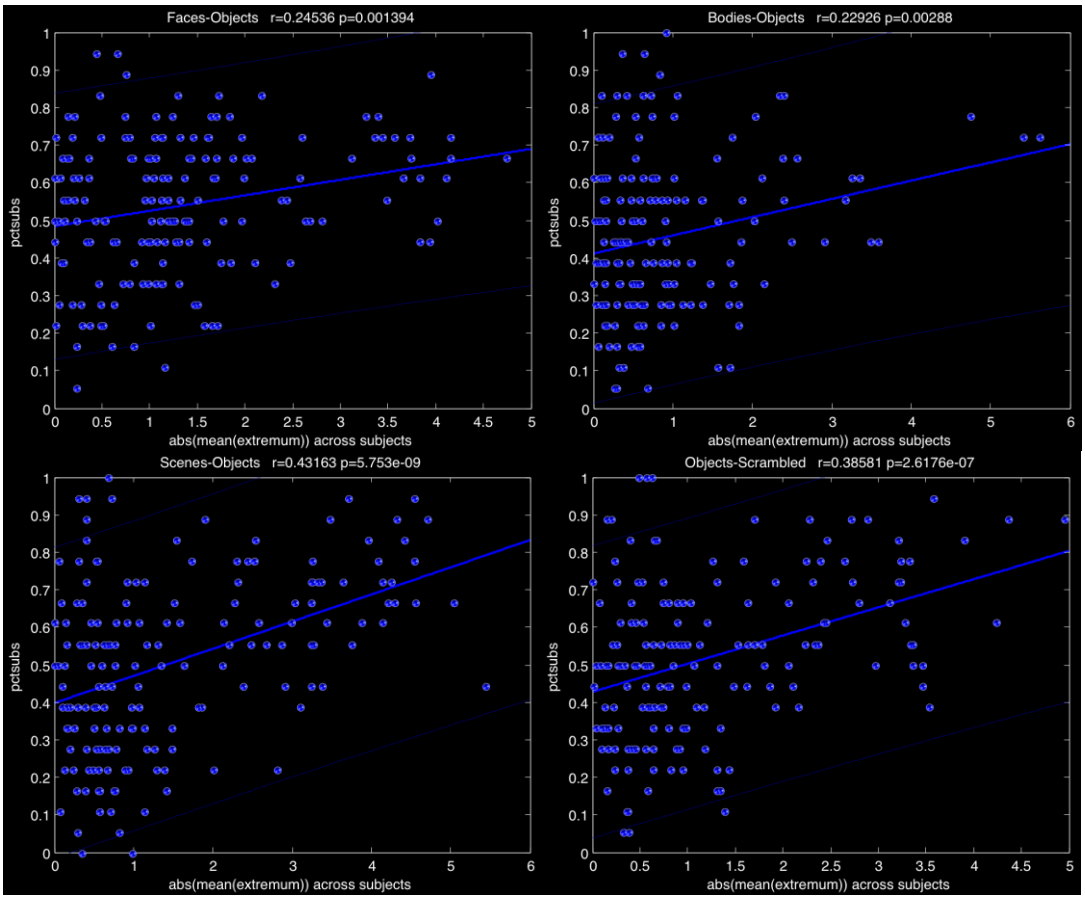

Figure 4. Prediction accuracies positively correlate with the functional selectivity of each region. Extremum absolute response values per region are averaged across subjects (x-axis) and plotted by the percentage of subjects that pass the random permutation benchmark for that region (y-axis). Regions with higher responses to the contrast, or greater selectivity for one visual category over another, tend to be the regions that are better predicted by connectivity.

A one-way ANOVA revealed that certain contrasts had significantly lower prediction errors across all gray matter voxels than other contrasts ($F(3)=14.47$, $p=2.18x10^{-7}$). The connectivity-based predictions for Bodies > Objects had significantly higher errors than each of the other contrasts (Bodies > Objects vs. each of: Faces > Objects t=10.00, p=1.54E-08; Scenes > Objects t=5.85, p=1.93E-05; Objects > Scrambled t=4.61, p=2.52E-04). Additionally, Faces > Objects and Scenes > Objects were significantly more accurate than Objects > Scrambled (t=3.88, p=1.21E-03; t=3.86, p=1.26E-03). Faces > Objects and Scenes > Objects prediction errors were not significantly different from one another. These results were replicated in group 2 ($F(3)=10.463$; p=4.31E-05; **Supplementary Table 2** for pair-wise post-hoc tests).

Supplementary Table 2. Group 2 post-hoc t-tests to identify which contrasts were better predicted by connectivity than others.

contrast 1	vs. contrast 2	p	t
Faces-Objects	Bodies-Objects	1.30E-04	-6.37
Faces-Objects	Scenes-Objects	2.30E-01	1.289
Faces-Objects	Objects-Scrambled	1.02E-01	-1.822
Scenes-Objects	Bodies-Objects	6.98E-06	-9.223
Objects-Scrambled	Bodies-Objects	9.44E-04	-4.822
Scenes-Objects	Objects-Scrambled	5.70E-03	-3.606

2. Final connectivity models account for much of the fMRI variance in each functional contrast.

Final models were built from the connectivity and functional data of all of the group 1 participants and the model fits (R^2) were calculated per anatomical region. These R^2 values reflect the proportion of fMRI variance that connectivity can account for across all of the voxels per parcel and across all of the subjects in group 1. Across the contrasts, the R^2 values ranged from nearly zero to more than 0.4. For each parcel and for each contrast, we calculated the absolute value of the mean extremum across subjects, and correlated these values with each parcel's R^2. Each contrast correlated positively and significantly (**Figure 5a**): Faces > Objects $r=0.42$, $p=1.2\times10^{-8}$; Bodies > Objects $r=0.27$, $p=4.4\times10^{-4}$; Objects > Scrambled $r=0.55$, $p=1.3\times10^{-14;}$ Scenes > Objects $r=0.65$, $p=2.6\times10^{-21}$. We also related the R^2 values with a second metric of functional selectivity: multivoxel pattern analysis accuracy (MVPA; see Haxby et al. 2001), which reflects the degree to which all voxels of a parcel are collectively able to differentiate each functional contrast. The R^2 values were positively and significantly correlated with MVPA accuracy (**Figure 5b**): Faces > Objects $r=0.34$, $p=5.7\times10^{-6}$; Bodies > Objects $r=0.38$, $p=5.7\times10^{-7}$; Objects > Scrambled $r=0.56$, $p=6.1\times10^{-15;}$ Scenes > Objects $r=0.56$, $p=5.0\times10^{-15}$. Thus, parcels with greater functional selectivity for a given functional contrast were better fit by models of connectivity.

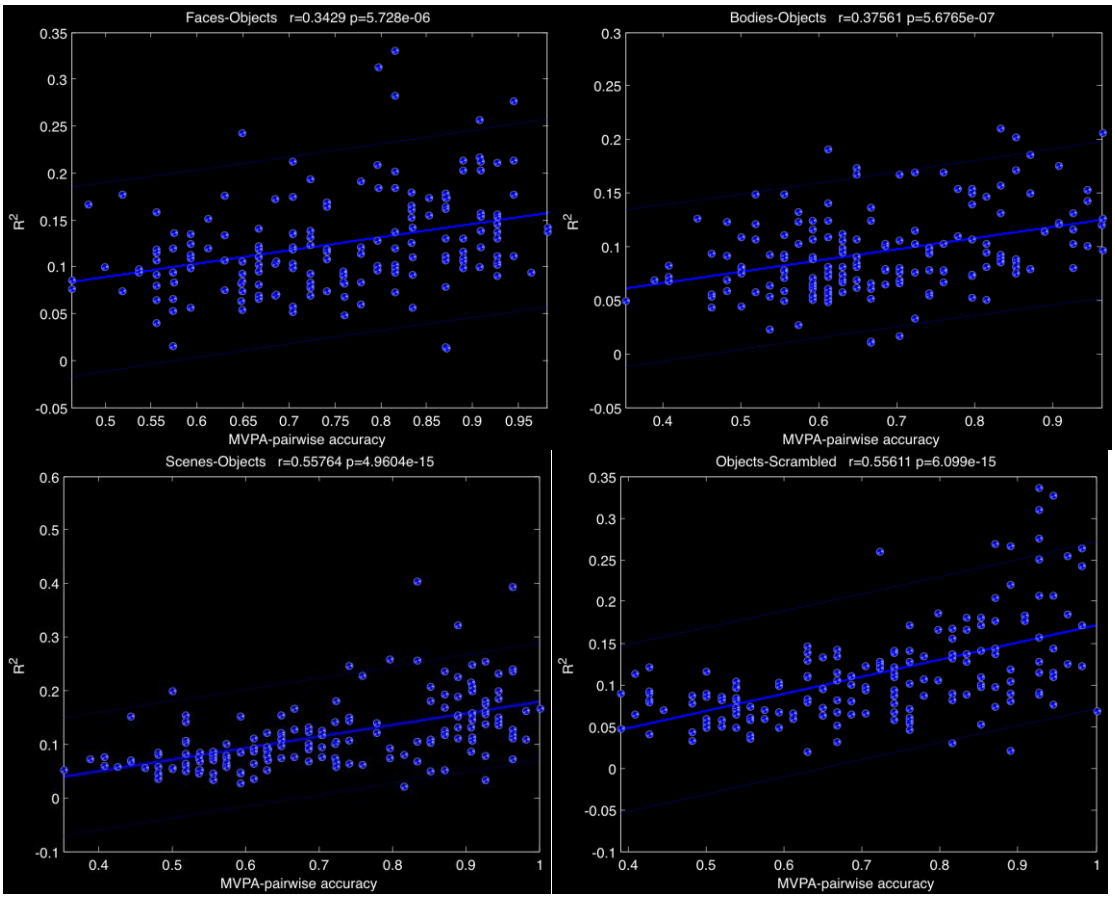

Figure 5. Final model fits also positively correlate with MVPA functional selectivity per anatomical parcel. The fits or R^2 values for the final models per anatomical region that were built from the connectivity and functional data of all group 1 participants, positively correlated with MVPA pairwise accuracies, which reflect the response selectivity of each parcel to each functional contrast (**a.** Faces > Objects, **b.** Bodies> Objects, **c.** Scenes>Objects, **d.** Objects>Scrambled). Parcels with better model fits of fMRI activity with connectivity were those parcels with greater functional selectivity for that functional contrast.

3. Connectivity-based predictions of functional contrasts are more accurate than group-average predictions of fMRI activity.

Since group-analyses are standard in neuroimaging, they were chosen as benchmark models that connectivity-based predictions should meet or exceed in order to be considered useful. We first evaluated prediction errors in each individual's native anatomy (in diffusion space). For each contrast, connectivity significantly outperformed the benchmark across all of the gray matter voxels of group 1 participants (MAE: Faces > Objects: T(17)=-14.368, p=6.12E-11; Bodies > Objects: T(17)=-26.488; p=2.91E-15; Scenes > Objects: T(17)=-12.859; p=3.47E-10; Objects > Scrambled: T(17)=-10.118; p=1.30E-08; see **Table 2** for MSE). The benchmark models also offered a way to evaluate the replicability of the results in a separate group of participants (group 2). We found that connectivity outperformed benchmark models across all gray matter voxels for all contrasts (Faces > Objects: T(9)=-6.687, p=8.99E-05; Bodies > Objects: T(9)=-22.274; p=3.51E-09; Scenes > Objects: T(9)=-7.915; p=2.41E-05; Objects > Scrambled: T(9)=-7.495; p=3.71E-05; see **Table 2** for MSE comparisons which yielded similar results).

Table 2. Mean prediction errors and benchmark comparisons. Mean prediction errors (± standard error across participants) across all anatomical parcels for predicted fMRI activation to each functional contrast by connectivity models and group-average benchmarks. T-statistic and p-values are also reported for each contrast for the comparison of connectivity vs. group-average models. Negative t-values indicate lower prediction error (higher accuracy) for connectivity than group-average.

	Faces-Objects	**Bodies-Objects**	**Scenes-Objects**	**Objects-Scrambled**
MAE				
Group 1				
Connectivity	0.657±0.014	0.771±0.006	0.649±0.021	0.708±0.014
Group	0.775±0.019	0.977±0.012	0.764±0.028	0.847±0.025
Connectivity-Group *t*	-14.368	-26.488	-12.859	-10.118
Connectivity-Group *p*	6.12E-11	2.91E-15	3.47E-10	1.30E-08
Group 2				
Connectivity	0.680±0.017	0.784±0.009	0.662±0.019	0.718±0.020
Group	0.797±0.030	1.004±0.017	0.783±0.023	0.858±0.033
Connectivity-Group *t*	-6.687	-22.274	-7.915	-7.495
Connectivity-Group *p*	8.99E-05	3.51E-09	2.41E-05	3.71E-05
MSE				
Group 1				
Connectivity	0.789±0.025	1.005±0.010	0.769±0.048	0.877±0.028
Group	1.012±0.050	1.549±0.037	0.979±0.079	1.174±0.070
Connectivity-Group *t*	-8.172	-19.33	-6.357	-6.798
Connectivity-Group *p*	2.73E-07	5.22E-13	7.16E-06	3.11E-06
Group 2				
Connectivity	0.816±0.039	1.034±0.020	0.780±0.039	0.863±0.041
Group	1.062±0.085	1.644±0.056	1.025±0.065	1.180±0.091
Connectivity-Group *t*	-4.69	-16.071	-5.884	-5.669
Connectivity-Group *p*	1.14E-03	6.19E-08	2.34E-04	3.06E-04

We also evaluated the performance of the connectivity models vs. group-average models within each of the fROIs typically associated with each functional contrast. These fROIs were independently-defined in another study and reflected the most probable locations of fROIs defined in each individual from a separate (large) group of subjects (see Julian et al. 2012). We calculated the percentage of subjects whose connectivity patterns significantly better predicted fMRI activation per voxel within each of these fROIs than a group-average prediction (within-subject voxel-wise comparisons within each fROI and thus $p > 0.05$ Bonferroni corrected for total number of fROIs by total subjects in both groups, i.e. 20x28). Almost all of the fROIs were significantly better predicted by connectivity patterns than a group-average in over 90% of subjects, with the exception of rFBA (**Figure 6a**). The results were replicated in group 2, with 100% of the subjects' fMRI activation better predicted by connectivity than by group in the rFFA, l and rOFA, rpcSTS, rSTS, l and rEBA, l and rPFS, l and rPPA, l and rRSC, l and rTOS, l and rLOC (**Figure 6b**).

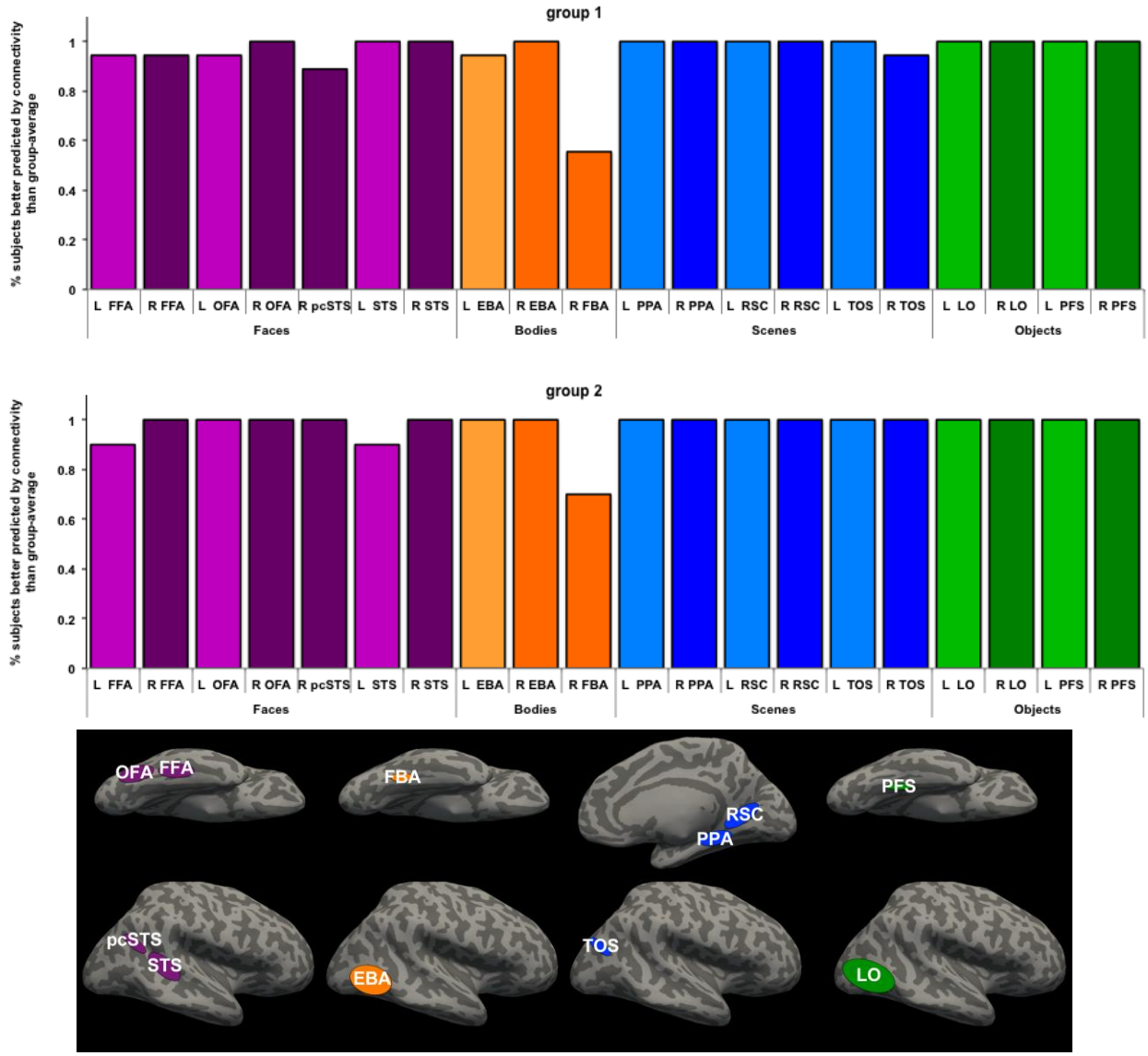

Figure 6. Predictive accuracy across subjects for connectivity vs. group-analysis benchmark. Within each of the fROIs, the percentage of subjects whose connectivity patterns better predict their activation patterns than a group-based prediction ($p < 0.05$ Bonferroni corrected for total number of fROIs by total number of subjects across both groups; i.e. 20x28) in **a.** the cross-validation group and **b.** replication test group. Lighter colors indicate left-hemisphere fROIs (some fROIs did not have a left-hemisphere counterpart).

4. Binarized maps of each individual's actual fROIs closely matched the prediction-based fROIs.

We binarized the connectivity-based fMRI predictions to create each of the fROIs per functional contrast and compared these predicted fROIs to each subject's actual fROI (created from the subject's actual fMRI image). The fROIs were created in each subjects' diffusion native space. Overall, predicted voxels were extremely close to the actual fROI. For example, each point in the predicted right FFA was on average less than 2 voxels away from the actual fROI, for both groups 1 and 2 (**Figure 7a, b**). Bilateral LO fROIs were some of the best predicted regions and right pcSTS and left STS were some of least accurate, but were still lower than 2.5 voxels away from the actual fROIs (**Figure 7a,b**). On average, face-selective fROIs were 1.98 voxels away, body-selective fROIs 1.56 voxels, scene-selective fROIs 1.70 voxels, and object-selective fROIs 1.64 voxels away from the actual fROIs. In group 2, which was the replication group that was naïve to building the connectivity-based models of fMRI, face-selective fROIs were 1.88 voxels away, body-selective fROIs 1.69 voxels, scene-selective fROIs 1.68 voxels, and object-selective fROIs 1.62 voxels away from the actual fROIs.

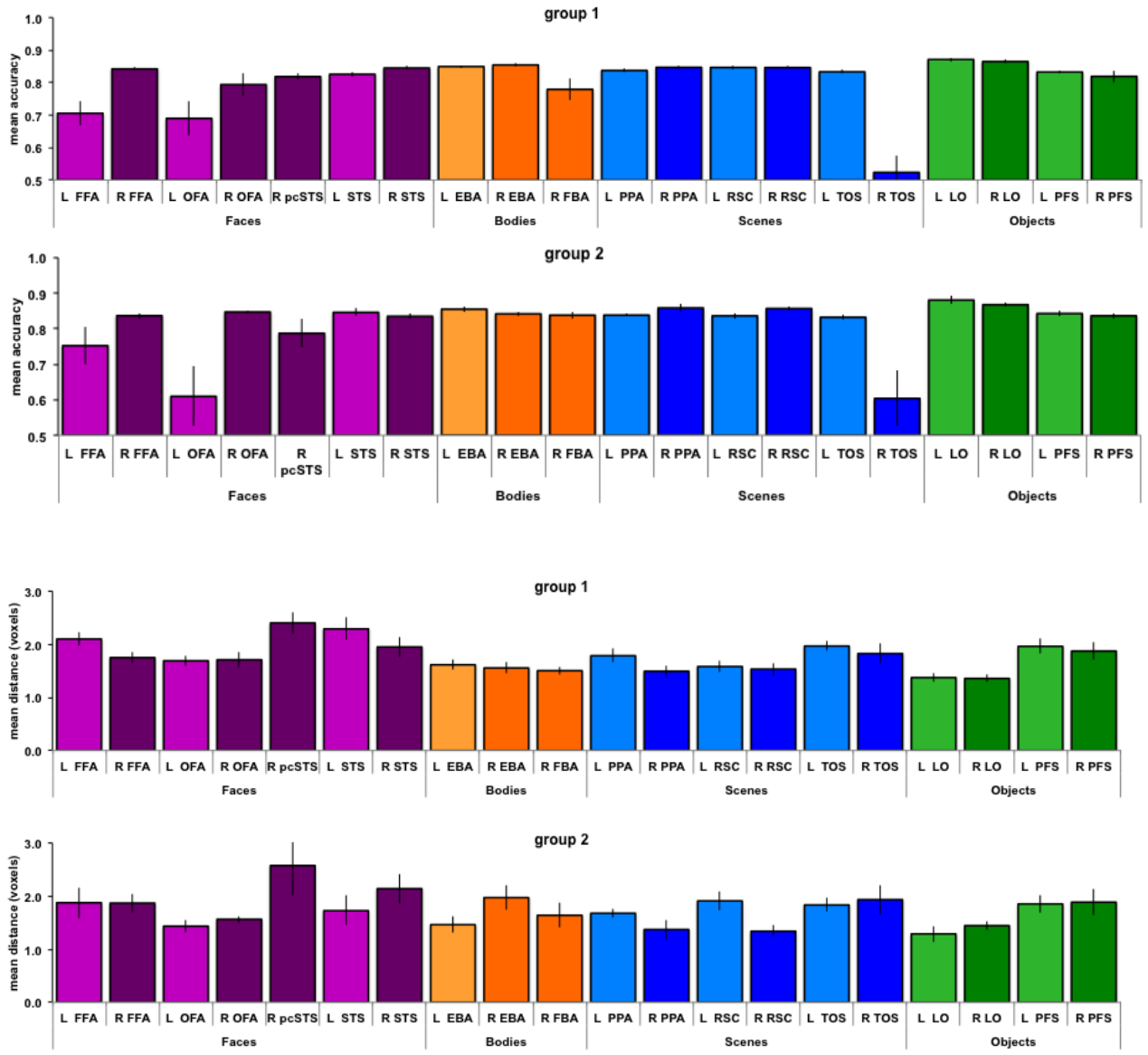

Figure 7. Bar plots of binarized actual and predicted fROIs. The mean and ste of accuracy is plotted for each fROI for both the cross-validation and replication groups. **a.** Accuracy measurements were constrained to the probabilistic fROI parcels (generated independently, see text). **b.** The mean Hausdorff distance was also calculated as the average distance from each point in the predicted fROI to the actual fROI. Lighter colors indicate left-hemisphere fROIs.

Discussion

We hypothesized that the anatomical connectivity of cortical voxels should be tightly coupled with that voxel's specialized neural responses to various visual stimulus categories. We tested this hypothesis by using a novel method of directly linking DWI and fMRI in the same individuals; this method had previously been used to predict voxel-wise face-selectivity in the fusiform from connectivity patterns alone. For each anatomically-defined parcel, we built connectivity models of function from a group of participants, applied the models to a new participant's DWI data to generate voxel-wise predictions of fMRI activity, and compared these predictions to the individual's actual fMRI activity.

We found that connectivity-based models of function were able to accurately predict fMRI activity to faces, objects, bodies, and scenes in new individuals using only their DWI connectivity patterns. For each of the four functional contrasts, the prediction accuracies were higher for cortical regions that had highly selective patterns of activation for that function. The final models of connectivity and function that were built from all the participants of group 1 accounted for more than twenty percent of the functional variance across all voxels of all subjects. The variance accounted for by connectivity per region was also significantly correlated with both the peak response per region and the MVPA accuracy for the region. Thus, voxels that make up a functionally-selective cortical region have distinct connectivity fingerprints that are predictive of functional selectivity; regions that are not functionally-selective do not have such unique voxel-wise connectivity fingerprints, at least for the functions tested here.

In addition, we compared the models to group averages, as a benchmark standard. For each function, connectivity outperformed the benchmark, both voxelwise across the whole brain, and within functionally-defined fROIs. We also found that all of the predicted fROIs were on

average less than two voxels to each individual's actual fROIs. We also replicated the findings in a separate group of participants (group 2) whose data were independent of the connectivity models.

These results refute alternatives to the hypothesis that unique connectivity patterns are coupled with functional selectivity. If all regions were equally well-predicted by connectivity (i.e. all regions pass random permutation testing) or there was no relationship between selectivity and predictability (i.e. no significant correlation between accuracy or R^2 with functional selectivity), then it would suggest that, as a rule, the principle predictor of selectivity (or lack thereof) is determined by patterns of connectivity. On the other hand, if we had found an inverse relationship with function (i.e. regions that are non-selective are best predicted, regions that are selective are worst predicted) it would suggest that the response of a functionally-selective region is determined mainly by intra-areal connectivity (intrinsic connections) and/or that the input or output of a region (its extrinsic connections) do not reflect the specialization of that region. While intra-areal connectivity is undoubtedly a large component of determining a region's functional responses, our analyses are specifically testing the role of extrinsic connections in determining cortical function. Although we cannot distinguish between input and output with DWI, we can conclude that functionally-specialized cortical regions are receiving or outputting specialized projections for function, at least with respect to high-level visual function.

It will be interesting to identify the limits of this approach across functional domains. The stimulus categories used in the present experiment represent some of the most robust and replicable of perceptual domains and thus it remains possible that this approach is best-suited for such robust domains. It may be unable to account for functional and inter-subject variability in more cognitive and perhaps less-robust tasks such as decision-making or emotional reappraisal.

Further, amassing a large database of functional tasks and their predictability through connectivity may be useful for predicting a variety of tasks in a single subject, all with a ten-minute diffusion scan.

These results suggest that functionally-selective brain regions are fundamentally specialized due to their characteristic patterns of connectivity. Further, the results demonstrate the use of DWI to delineate boundaries of regions that are specialized for particular behavioral or neural functions, and suggest that a ten-minute DWI scan can predict function more accurately than current benchmark methods and within two voxels of the individual's actual fROIs. In addition to fundamentally enhancing our current understanding of structure-function relationships in the brain, the method we used here has useful clinical applications; for example, it can be used to characterize neural responses in patient populations who cannot be awake during an fMRI scan (i.e. low-functioning autism, comatose patients) or for guiding pre-surgical planning.

References

Johansen-Berg, H., Behrens, T. E. J., Robson, M. D., Drobnjak, I., Rushworth, M. F. S., Brady, J. M., Smith, S. M., Higham, D. J., & Matthews, P. M. (2004). Changes in connectivity profiles define functionally distinct regions in human medial frontal cortex. *Proc. Natl. Acad. Sci. U. S. A.*, *101*(36), 13335–40.

Frost, M. A., & Goebel, R. (2012). Measuring structural-functional correspondence: spatial variability of specialised brain regions after macro-anatomical alignment. *NeuroImage*, *59*(2), 1369–81. doi:10.1016/j.neuroimage.2011.08.035

Saxe, R., Brett, M., & Kanwisher, N. (2006). Divide and conquer: a defense of functional localizers. *NeuroImage*, *30*(4), 1088–96; discussion 1097–9. doi:10.1016/j.neuroimage.2005.12.062

Saygin, Z. M., Osher, D. E., Koldewyn, K., Reynolds, G., Gabrieli, J. D. E., & Saxe, R. R. (2012). Anatomical connectivity patterns predict face selectivity in the fusiform gyrus. *Nat. Neurosci.*, *15*(2), 321–7. doi:10.1038/nn.3001

Ungerleider, L. G., & Mishkin, M. (1982). Two cortical visual systems. In D. Ingle, M. A. Goodale, & R. J. W. Mansfield (Eds.), *Analysis of Visual Behaviour* (pp. 549–586). Cambridge: MIT Press.

Felleman, D. J., & Van Essen, D. C. (1991). Distributed hierarchical processing in the primate cerebral cortex. *Cereb. Cortex, 1*(1), 1–47.

Tsao, D. Y., Freiwald, W. A., Tootell, R. B. H., & Livingstone, M. S. (2006). A cortical region consisting entirely of face-selective cells. *Science*, *311*(5761), 670–4. doi:10.1126/science.1119983

Colby, C. L., & Goldberg, M. E. (1999). Space and attention in parietal cortex. *Annu. Rev. Neurosci.*, *22*(1), 319–49. doi:10.1146/annurev.neuro.22.1.319

Kanwisher, N., & Dilks, D. D. (n.d.). The Functional Organization of the Ventral Visual Pathway in Humans. In J. S. Werner & L. M. Chalupa (Eds.), *The New Visual Neurosciences*. Cambridge: MIT Press.

Reese, T.G., Heid, O., Weisskoff, R.M. & Wedeen, V.J. Reduction of eddy-current-induced distortion in diffusion MRI using a twice-refocused spin echo. Magn. Reson. Med. 49, 177–182 (2003).

Behrens et al. 2007 Fischl, B. et al. Automatically parcellating the human cerebral cortex. Cereb. Cortex 14, 11–22 (2004).

Fischl, B. et al. Whole brain segmentation: automated labeling of neuroanatomical structures in the human brain. Neuron 33, 341–355 (2002).

Desikan, R.S. et al. An automated labeling system for subdividing the human cerebral cortex on MRI scans into gyral based regions of interest. Neuroimage 31, 968–980 (2006).

Behrens, T.E., Berg, H.J., Jbabdi, S., Rushworth, M.F. & Woolrich, M.W. Probabilistic diffusion tractography with multiple fibre orientations: what can we gain? Neuroimage 34, 144–155 (2007).

Pitcher, D., Dilks, D.D., Saxe, R.R., Triantafyllou, C. & Kanwisher, N. Differential selectivity for dynamic versus static information in face-selective cortical regions. Neuroimage 56, 2356–2363 (2011).

Haxby, J., Gobbini, M., Furey, M., Ishai, A., Schouten, J., and Pietrini, P. (2001). Distributed and overlapping representations of faces and objects in ventral temporal cortex. Science 293, 2425–2430.

Julian, J. B., Fedorenko, E., Webster, J., & Kanwisher, N. (2012). An algorithmic method for functionally defining regions of interest in the ventral visual pathway. NeuroImage, 60(4), 2357–64. doi:10.1016/j.neuroimage.2012.02.055

G.M. Postelnicu, L. Zöllei, B. Fischl: "Combined Volumetric and Surface Registration", IEEE Transactions on Medical Imaging (TMI), Vol 28 (4), April 2009, p. 508-522

Zöllei, L., A. Stevens, K. Huber, S. Kakunoori, B. Fischl: "Improved Tractography Alignment Using Combined Volumetric and Surface Registration", NeuroImage 51 (2010), 206-213

Yendiki A, Panneck P, Srinivasan P, Stevens A, Zöllei L, Augustinack J, Wang R, Salat D, Ehrlich S, Behrens T, Jbabdi S, Gollub R and Fischl B (2011). Front. Neuroinform. 5:23. doi: 10.3389/fninf.2011.00023

Chapter 4

Functionally relevant networks for predicting visual categorical responses.

We used a novel method of predicting function from DWI connectivity to explore the functional connectomics for different visual categorical representations. Diffusion-weighted images and fMRI images were acquired from two groups of healthy subjects. Probabilistic diffusion tractography was performed from each anatomically-defined parcel to all other anatomical parcels. For each parcel, we modeled the fMRI data as a function of connection probability using linear regressions. Connectivity models of functional activation to visual categories were used to identify the subset of connections that best predicted voxel-wise functional activation, or the functionally relevant network (FRN), for each functional contrast for each anatomically-defined parcel. By comparing the FRNs across visual categorical domains, we found that there are unique sets of connections for predicting different functions. Object and scene representations shared some aspects of the FRNs with one another, while body and face FRNs were similar to one another and dissimilar to object and scene FRNs. This approach demonstrates the prospect of using anatomical connectivity to predict functional responses to a variety of stimuli, encouraging the assembly of a database of model coefficients for numerous other conditions. Such a database would enable a researcher to estimate functional responses to a range of experimental conditions from a single diffusion scan that lasts only about 10 minutes.

Introduction

Structural connectivity is among the most important constraints on a neural network since it restricts and defines the sort of information that can be processed. The functional responses of a voxel should therefore be strongly influenced by its pattern of connectivity; correspondingly, patterns of connectivity should be highly predictive of function.

Not all the connections are equally influential for a particular mental, however. The relevant input/output patterns are probably unique for small variations in function. For example, less than 5% of the inputs to macaque primary visual cortex, V1, arrive from the optic radiations, which are undeniably critical agents to visual responses in V1. In order to better understand the mechanisms underlying brain function, we need to identify the critical connections that underlie function, and which connections 'weigh in' more for a particular function.

By testing fMRI responses to a variety of functional domains, we have discovered that there exists a tight relationship between connectivity and function across diverse visual domains, such that a voxel's unique connectivity patterns (its connectivity fingerprint) can predict that voxel's functional selectivity to visual representations of faces, scenes, objects, and bodies. However, each connection has a different relative weight in producing a given function of that region, which is in a way, the functionally-relevant network of that region, or functional connectomics in general. We now explore these networks across the different visual categorical domains and investigate what the functionally-relevant connections are, and what makes a voxel's pattern of connections unique for a particular function, or general for all visual functions.

Methods

Participants.

The study included 18 participants (mean age=26.4, 7M:11F) who were recruited from the greater Boston area. Participants were screened for history of mental illness, gave written informed consent, and were compensated at $30 per hour. The study was approved by the Massachusetts Institute of Technology and Massachusetts General Hospital ethics committees.

DWI acquisition parameters and tractography.

DWI data were acquired using echo planar imaging (64 slices, voxel size 2 × 2 × 2 mm, 128 × 128 base resolution, diffusion weighting isotropically distributed along 30 directions, *b*-value 700 s mm^{-2}) on a 3-T Siemens scanner with a 32-channel head-coil (Reese et al. 2003). A high resolution (1 mm^3) three-dimensional magnetization-prepared rapid acquisition with gradient echo (MPRAGE) scan was acquired on these participants.

Automated cortical and subcortical parcellation was performed in each participant's T1 scan, using the Desikan-Killiany atlas (Desikan et al. 2006) from Freesurfer 5.1 (Fischl et al. 2002, 2004) to define 86 cortical and subcortical regions. Automated segmentation results were reviewed for quality control and were then registered to each individual's diffusion images and used as the seed and target regions for fiber tracking. The resulting cortical and subcortical targets were then checked and corrected for automatic parcellation or segmentation errors if necessary. The principal diffusion directions were calculated per voxel, and probabilistic diffusion tractography was carried out using FSL-FDT (Behrens et al. 2008) with 5,000 streamline samples in each seed voxel to create a connectivity distribution to each of the target regions, while avoiding a mask consisting of the ventricles. Each of the 86 regions was used as a seed region and tractography was carried out to all 85 remaining regions, or targets. Thus, every

voxel within each parcel is described by a vector of connection probabilities to each other brain region. Note that the anatomical parcels used here were larger than the ones used in Chapter 3, but since they produced the same results as the 169 regions, they were used for evaluating the predictive networks since there are fewer regions and the parcel-naming conventions are more parsimonious.

fMRI acquisition parameters and analysis.

Stimuli for the fMRI consisted of 3-s movie clips of faces, bodies, scenes, objects and scrambled objects. Movies of faces and bodies were filmed against a black background and framed to reveal just the faces or bodies of seven individuals, shown one at a time. Scenes consisted primarily of pastoral scenes filmed through a car window while driving slowly through the countryside or suburb. Objects were selected specifically to minimize any suggestion of animacy of the object itself or of an invisible actor pushing the object. Scrambled object clips were constructed by dividing each object movie clip into a 15 × 15 box grid and spatially rearranging the location of each of the resulting boxes. Pilot testing indicated that a contrast of the response for moving faces versus moving objects identified the same FFA as that identified in a standard static localizer. Further studies show that the FFA responds similarly to movies of faces as to static snapshots of faces (Pitcher et al. 2011).

Functional data were acquired over four block-design functional runs (gradient echo sequence 2,000 ms TR, 30 ms TE, 90° flip, 234 volumes, 3 × 3 × 3 mm voxel size). Each functional run contained three 18-s fixation blocks at the beginning, middle and end of the run. During these blocks, a series of six uniform color fields were presented for 3 s each. Each run also contained two sets of five consecutive stimulus blocks (faces, bodies, scenes, objects or scrambled objects) sandwiched between these rest blocks, resulting in two blocks per stimulus

category per run. Each block lasted 18 s and contained six 3-s movies clips from each of the five stimulus categories. The order of stimulus category blocks in each run was palindromic, and specific movie clips were chosen randomly to be presented during the block. Participants were asked to passively view the stimuli.

Functional data were analyzed with FSL software (http://www.fmrib.ox.ac.uk/fsl/). Images were motion corrected, smoothed (5 mm Gaussian kernel, full width at half maximum) and detrended, and were fit using a standard gamma function (= 2.25 and = 1.25). Data were not spatially normalized. Statistical modeling was then performed using a general linear model on the preprocessed functional images. Next, *t*-maps corresponding to each contrast of interest were overlaid on each participant's high-resolution anatomical image. The contrasts were as follows: Faces > Objects, Bodies > Objects, Scenes > Objects, Objects > Scrambled objects.

Each participant's functional image for each contrast was registered to his or her diffusion-weighted image. Because we were interested in predicting relative activation values that were independent of task-specific parameters such as the degrees of freedom, we standardized the *t*-statistic values across all gray matter parcels per participant. For each anatomical parcel, the mean functional value across the brain was subtracted from each voxel and divided by the standard deviation. The standardized value per voxel was then used for the subsequent regression models, which were built per region. Thus, every voxel is now also described by a vector of *t*-statistics for each functional contrast.

Regressions.

Analyses were performed on subject-specific anatomy, rather than extrapolation from a template brain. For the regression models, each observation was an individual voxel in native space, and there was no identifying or matching of spatial location of voxels across participants. Further, the model was blind to the participant each voxel belonged to.

The model was designed as follows: every voxel of the modeled region has a neural response to a given functional contrast, which collectively make up a response vector. Every voxel also has a vector of connection probabilities to each other brain region, which collectively make up a matrix of regressors. The predictive relationship between connectivity and neural activity was inferred via linear regression from all of the subjects resulting in a set of predictive coefficients. For each anatomical parcel and each functional contrast, we generated a final linear regression model from all subjects' connectivity and fMRI data (from group 1 of Chapter 3).

Predictive networks between contrasts

The model coefficients of each parcel represent the predictive relationship between connectivity and neural activity. Since we modeled all parcels, we can assess not only which regions are predictive of a particular parcel, but also which regions that parcel predicts. For each functional contrast, we determined which regions were significant predictors for each other region, preserving the sign of the original coefficient, in order to produce an 86x86 square affinity matrix. To illustrate, a row of this matrix represents a single parcel, and its columns reflect whether each other region significantly predicts this parcel's neural activity: significant positive predictors are represented by ones, significant negative predictors are represented by negative ones, and nonsignificant predictors are represented by zeroes. We depict this matrix as

a network, with predictors as sources and the regions that they predict as sinks (i.e. arrows originate from predictors and point towards the regions that they predict).

Due to the massive complexity of such a depiction, we also generated simpler subnetworks that more clearly demonstrate key features of the full network. Since each of the functional contrasts involves visual perception, we eliminated all nodes that are not part of the ventral visual stream, leaving only occipital and temporal targets. The resulting network is still quite complex and difficult to visually parse, and so we focused our analyses to only the bidirectional and positive edges.

Results

For each region, we trained a linear regression on the voxel-wise fMRI and connection probabilities across subjects, and identified the predictive networks of function for each anatomical parcel. We started by first focusing on those parcels that encapsulated the relevant functional regions of interest (fROIs) for each functional domain. Then we evaluated all occipitotemporal connections that were predictive of each of the four functional domains and compared them across different functions.

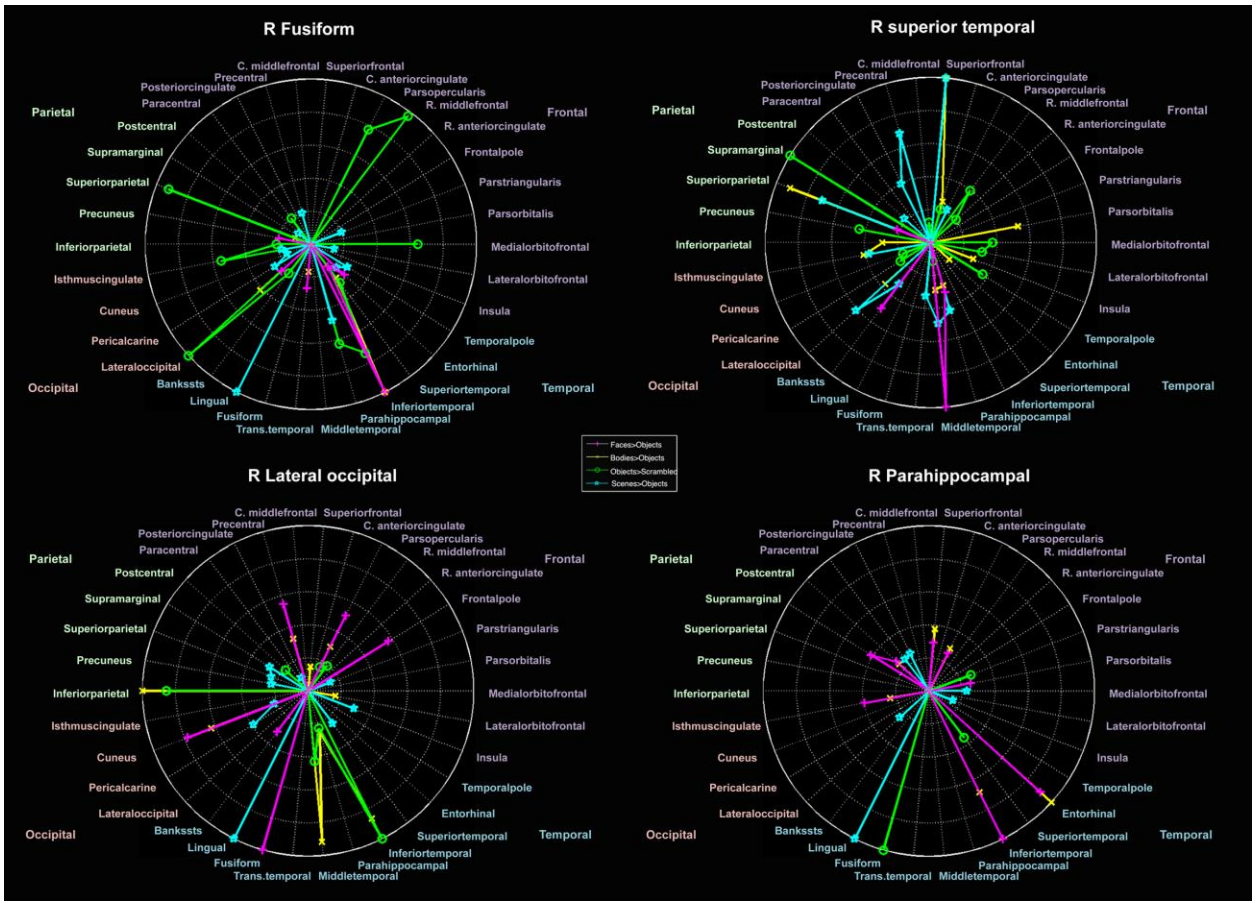

Figure 8. Functionally-relevant networks (FRNs) for anatomically-defined regions.

Significant predictors of fMRI activity to faces, bodies, or objects are plotted by their relative contributions to predicting each category (ipsilateral connections only). **a.** The right fusiform has a general FRN for responses to objects, but much more specific FRN for bodies and faces. **b.** The right superior temporal sulcus also has a specific FRN for responses to faces, but the FRNs for bodies and objects include more targets, suggesting that they may be more general. **c.** In contrast, right lateral occipital has FRNs that are specific for all categories. Some aspects of the FRN are shared between categories (i.e. connectivity with inferiortemporal, middletemporal, parahippocampal for bodies and objects) while others are unique to a particular category, such as fusiform connectivity for predicting face responses in lateral occipital. **d.** The right

parahippocampus has a more selective FRN for scenes than for faces and bodies, which in turn share many of the same targets with one another but not with the scene FRN.

Predictive networks of function were different for each functional contrast.

We explored the regions that significantly contributed to predicting fMRI activity for each contrast, or the functionally-relevant networks (FRNs) per anatomical region. The Desikan-Killiany atlas (Desikan et al. 2006) was used for these analyses for simpler interpretation of the results (see Methods). We identified the FRNs for four occipitotemporal anatomical parcels that are most commonly reported to encapsulate the functionally-selective fROIs: fusiform, superior temporal sulcus, parahippocampal gyrus, and lateral occipital cortex. We compared the FRNs across the different functional contrasts to determine their relative sparsity (i.e. only a few regions make a significant contribution to predicting function in that region) vs. generality (i.e. many brain regions contribute to functional predictions). The fusiform reliably encapsulates the FFA and FBA fROIs, selective for faces and bodies respectively, so we compared the FRNs for faces and bodies to those of objects and scenes in this region. We found that the right fusiform was quite sparse in its FRN for faces and bodies but distributed for objects (**Figure 8a**). We also found that the right fusiform's responses to faces can be predicted from its connections with inferior temporal, superior temporal, and other temporal targets, and the lateral occipital cortex (which houses the face-selective OFA). Functional responses to bodies in this region can be predicted via a similar fingerprint, with a few exceptions. The FRNs for faces and bodies in the fusiform seem to be sparser and generally constrained to the occipitotemporal targets, while the FRNs for objects and scenes seem to be more distributed across the cortex. Similarly, the right superior temporal sulcus, which encapsulates the STS fROI, had sparse FRNs for faces which were also constrained to occipitotemporal regions. However, the FRN for bodies was not constrained only to occipitotemporal cortex, but rather, was distributed across the cortex much like the FRNs for objects and scenes (**Figure 8b**).

In contrast, right lateral occipital cortex, which usually houses the object-selective LOC, face-selective OFA, and body-selective EBA, was generally quite distributed in its FRN, regardless of the visual category (**Figure 8c**). Some aspects of the FRN were shared between categories (i.e. connectivity with inferiortemporal, middletemporal, parahippocampal for bodies and objects). Other aspects of the FRN were unique to a particular category, such as fusiform connectivity for predicting face responses in this parcel. The parahippocampus usually houses the PPA and its FRN for scenes was more unique than the other categories and did not share many targets with faces and bodies, while faces and bodies shared many of the same components of the FRNs with one another (**Figure 8d**).

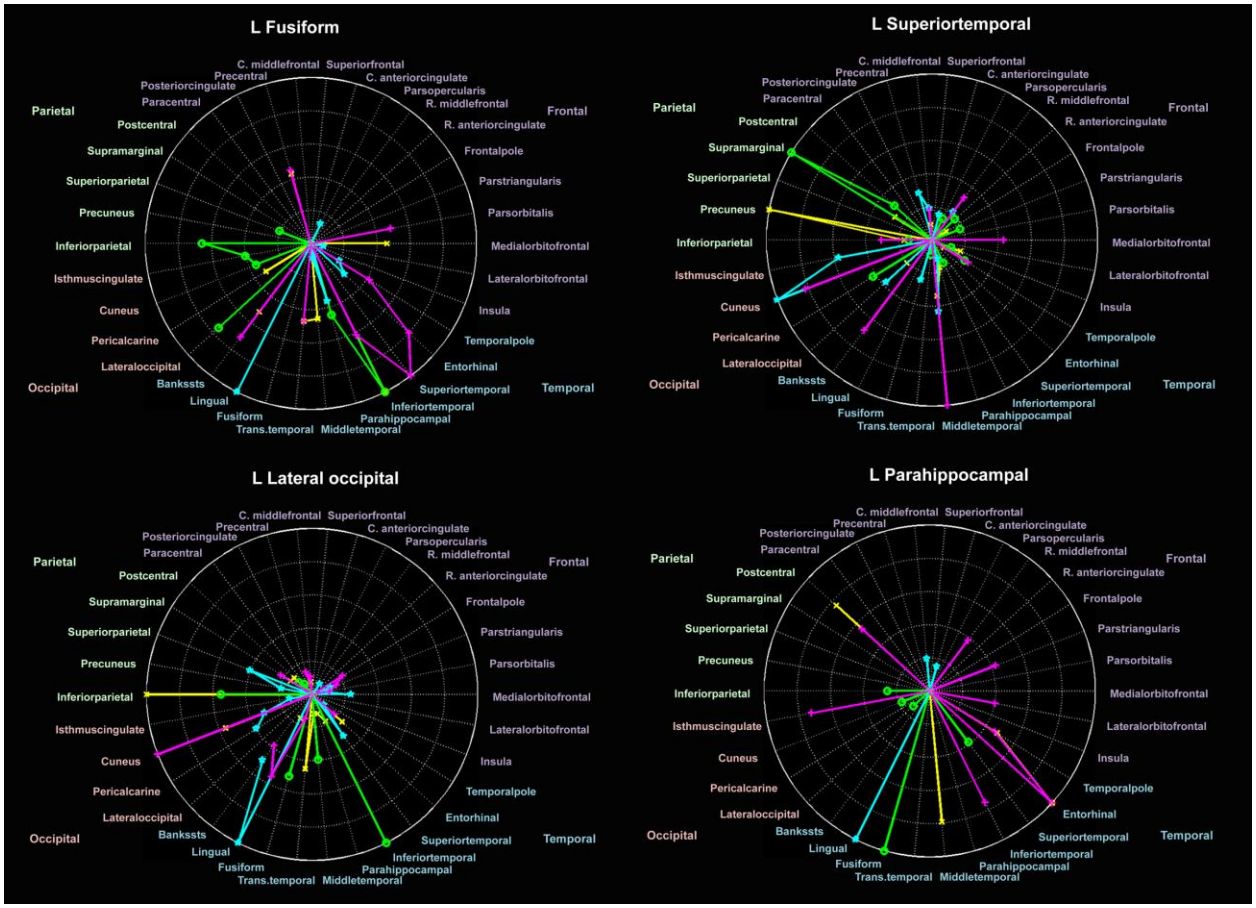

Supplementary Figure 2. Functionally-relevant networks for left-hemisphere anatomically-defined regions. a. The left-hemispheric fusiform was selective in its FRNs to faces and bodies, but still shared some of the same targets as the FRNs to objects. **b.** The left superior temporal sulcus had selective face FRNs, but shared many components with body and object FRNs, and was less selective than its right-hemisphere counterpart (see Figure 9). **c.** Left lateral occipital cortex had few FRN components shared between the functional contrasts, which were different than the right-sided parcel (see Figure 9). **d.** The left parahippocampal cortex was selective and shared few components of the scene FRN with the other contrasts.

The left hemisphere anatomical parcels exhibited similarly selective FRNs as their right counterparts, with some small differences. The left-hemispheric fusiform and superior temporal sulcus anatomical parcels were less sparse in their FRNs to faces and bodies, and faces respectively, which may reflect the observation that the functionally-selective fROIs are usually right-lateralized (**Supplementary Figure 2a,b**). Left lateral occipital cortex showed a slightly different pattern than its right counterpart, with fewer FRN components shared between the functional contrasts (**Supplementary Figure 2c**). The left parahippocampal cortex displayed a broader FRN for scenes than the right hemisphere but also shared few common targets with the other functional contrasts, thus reflecting the FRN's sparseness (**Supplementary Figure 2d**).

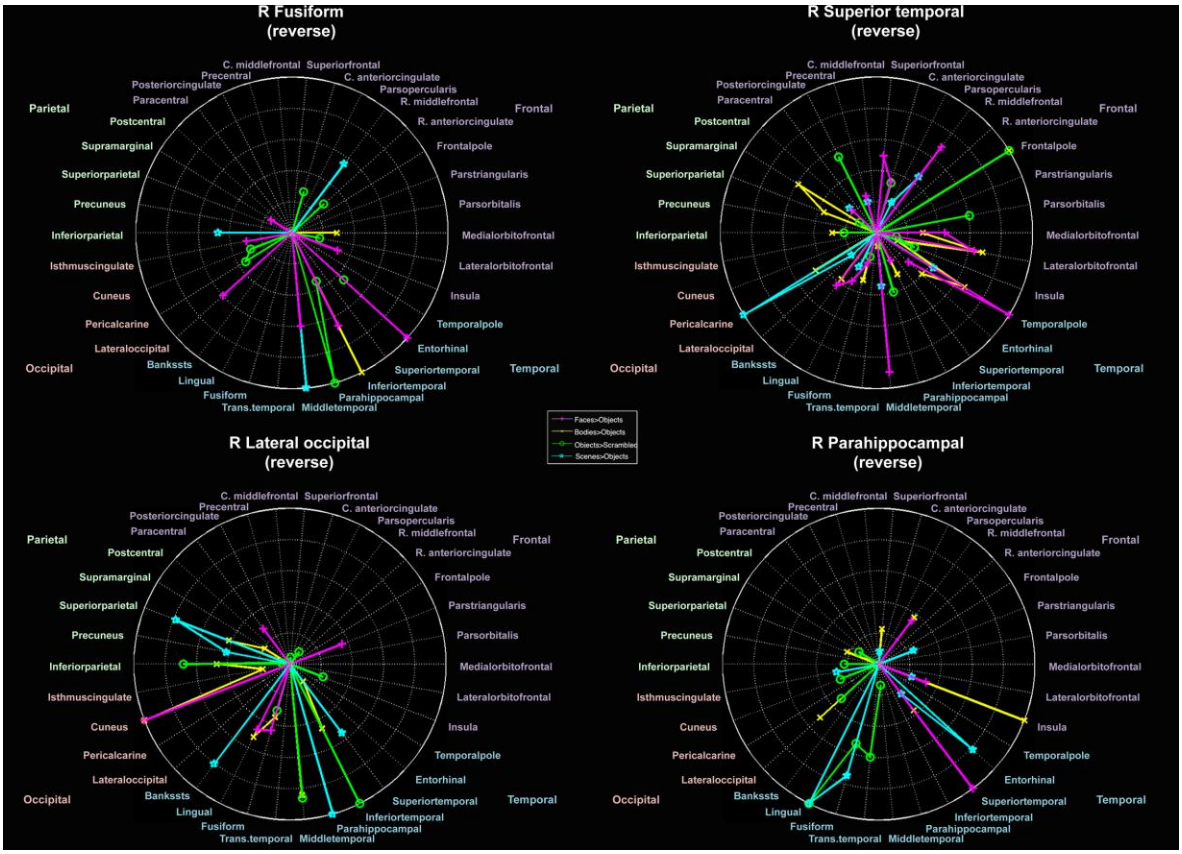

Figure 9. Reverse FRNs for anatomically-defined regions. Four occipitotemporal anatomical parcels are plotted by their relative contributions in predicting each category in each of the other anatomical parcels across the cortex (ipsilateral connections only). **a.** Fusiform is predictive of function for many different cortical parcels, which are in turn significant predictors of function in the fusiform. For face and body-selectivity, however, these regions are not only constrained to occipitotemporal regions, as they were for the "forward" FRNs. **b.** Superior temporal sulcus is quite distributed in which regions it was predictive for, especially for face-selectivity, which is again in contrast to its forward FRN. **c**. Lateral occipital cortex is predictive of face-, object-, body-, and scene-selectivity in many of the same regions that composed lateral occipital's forward FRN. **d.** The parahippocampus' reverse FRN for scenes shares many of the same regions as the other categories, and does not only include the same targets as its forward FRN**.**

We also analyzed the "reverse" FRNs, which depict the degree to which a particular region predicts all other regions, again comparing fusiform, STS, LO, and PHG (**Figure 9**). Fusiform was predictive of function across many different parts of cortex, including occipitotemporal, parietal, and frontal regions (see **Figure 8a** vs. **Figure 9a**). For face and body-selectivity, however, these regions were not only constrained to occipitotemporal regions, as they were for the "forward" FRNs. In other words, fusiform face- and body-selectivity was predicted by a more local network of occipitotemporal regions, which were in turn reciprocally predicted by their fusiform connectivity. The superior temporal sulcus was even more distributed than the fusiform in its predictiveness of functional selectivity across the brain; this was especially evident for face-selectivity (**Figure 9b**), suggesting that this region's role in the extended face-network may be to inform higher-order processing related to face representations. Lateral occipital cortex was predictive of face-, object-, body-, and scene-selectivity for the same regions that were predictive of lateral occipital's forward FRN (**Figure 9c**). In conjunction with the face-selectivity findings in the other two regions (LO, STS), these results suggest a hierarchical network of regions whereby lateral occipital is most local in its network (i.e. the same connections that predict its function are the regions for which it is predictive), fusiform is somewhat less local (most but not all of the connections are with the same regions), and superior temporal sulcus is predictive of face-selectivity in a multitude of regions while only getting predictive 'input' from a local network.

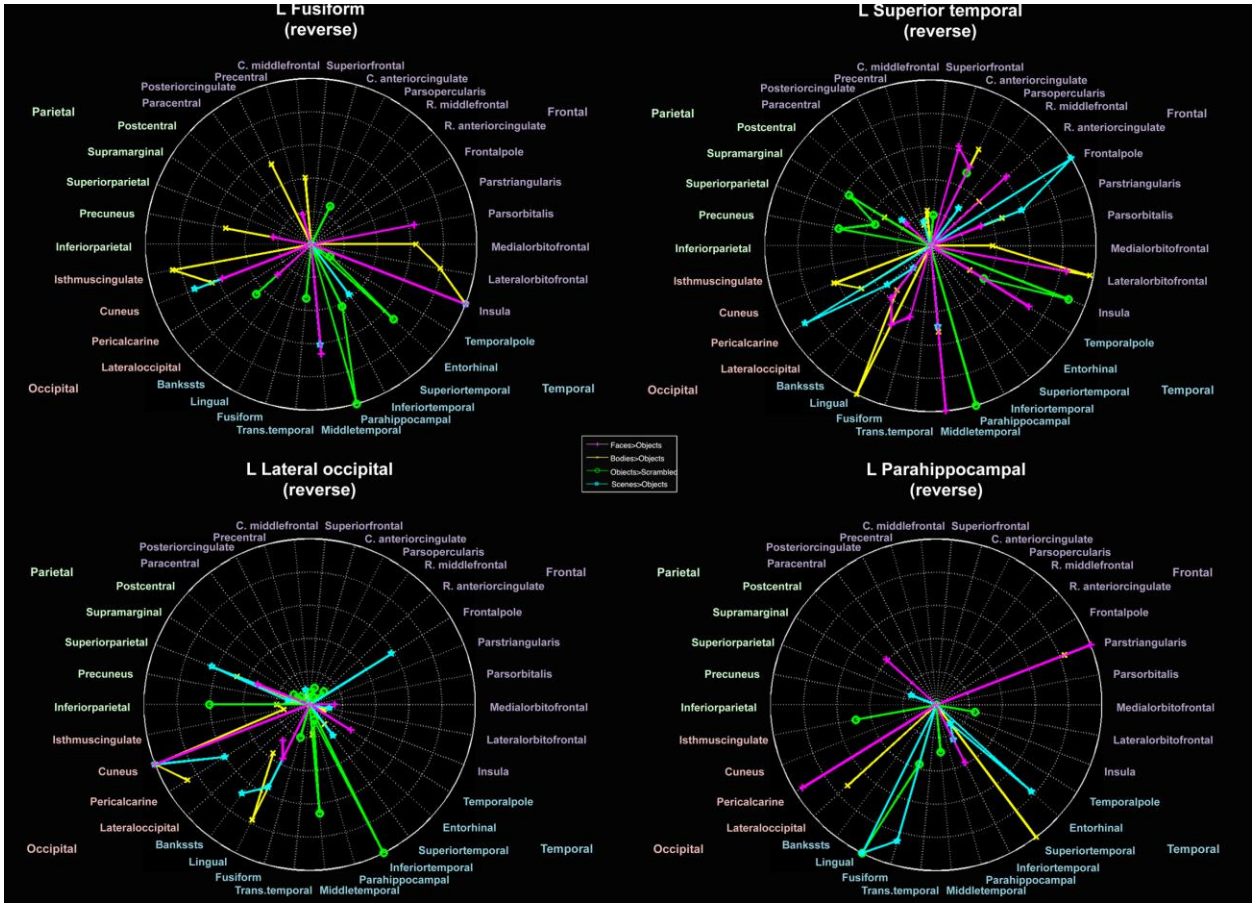

Supplementary Figure 3. Reverse FRNs for left-hemisphere anatomically-defined regions.

a. The left-hemispheric fusiform was selective in its reverse FRNs to faces and bodies, but still shared some of the same targets as the FRNs to scenes. **b.** The left superior temporal sulcus had distributed reverse FRNs for face and shared some components with body, object, and scene FRNs. **c.** Left lateral occipital cortex had few reverse FRN components shared between the functional contrasts, but these were many of the same regions that composed its forward FRNs (regions that lateral occipital is predictive of function for are the same regions that predict its function). **d.** The left parahippocampal cortex was quite sparse in its reverse FRNs and each category shared few components of the reverse FRNs of other contrasts.

The right parahippocampus' reverse FRN for scenes shared many of the same regions as the other categories, and included many of the targets in its forward FRN as well as several others (**Figure 9d**). By contrast, the left parahippocampal cortex was quite sparse in its reverse FRNs and each category shared few components of the reverse FRNs of other contrasts (**Supplementary Figure 3**). The other left-hemisphere reverse FRNs were distributed across the cortex and shared many of the same components across contrasts, thus exhibiting less sparse reverse FRNs than their right-hemisphere counterparts.

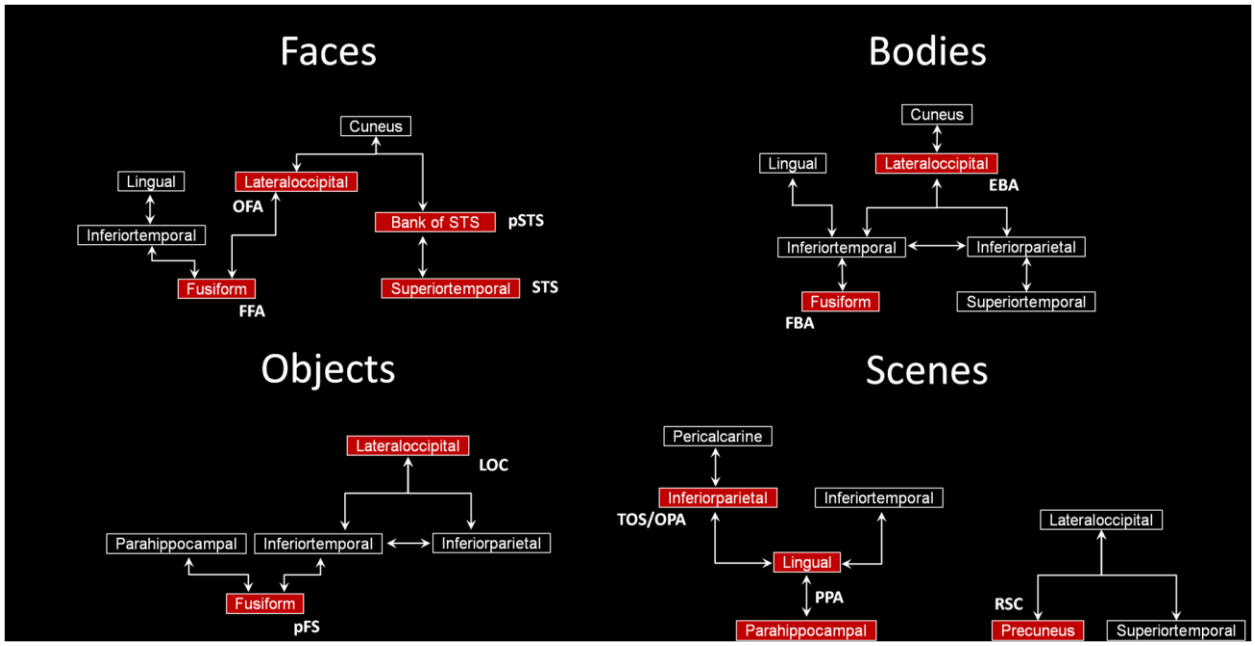

Figure 10. FRNs for occipitotemporal regions. The nodes of these subnetworks are the occipitotemporal parcels, and the edges include the bidirectional and positive significant predictors. Regions that lack any edges to these nodes are omitted. FRNs are depicted for **a.** faces, **b.** bodies, **c.** objects, and **d.** scenes.

We next analyzed the FRNs across regions and within contrasts, which can be depicted as a network, with predictors as sources and the regions that they predict as sinks (i.e. arrows originate from predictors and point towards the regions that they predict, **Figure 10**). Since each of the functional contrasts involves visual perception, we limited this analysis to occipital and temporal targets, which produced a much more parsimonious subnetwork. For this analysis, we focused on bidirectional and positive edges, because when connectivity between two regions is mutually positively predictive, it follows that the most functionally selective voxels are particularly connected to one another compared to the rest of the region.

The face FRN (**Figure 10a**) reveals that the voxels of lateral occipital that are connected to fusiform voxels are specifically face-selective; non-face-selective voxels are not connected between these regions, and furthermore, connectivity between the regions are not mutually influential for any of the other contrasts. This is especially intriguing since fusiform houses the FFA while lateral occipital houses the OFA. Further, the bank of STS (pSTS) has a similar relationship with superior temporal (STS). These interactions are also independent, which suggests parallel face-processing pathways. Both lateral occipital and bank of STS are connected to cuneus, which is composed of early visual areas such as V1, V2, and some other early extrastriate cortex.

The primary body-responsive fROIs include EBA in lateral occipital and FBA in fusiform. Although these are the same regions which house the face-selective OFA and FFA, the body FRN (**Figure 10b**) demonstrates that the body-selective voxels in these regions are not especially connected compared to connectivity between voxels of the rest of the regions. However, this does not imply that these regions are not directly connected; it merely indicates that their connections are not special for body-selective voxels and thus suggests that these

connections may not specifically carry information related to the processing of body perception. However, the body-selective voxels of these regions are indirectly connected through inferior temporal and inferior parietal cortices.

The object FRN (**Figure 10c**) contains the same motif as the body FRN: the functionally-selective connectivity between lateral occipital and fusiform is indirect and connects through inferior temporal and inferior parietal cortices. The scene FRN (**Figure 10d**) reveals two parallel subnetworks. The first includes inferior parietal, which contains the occipital place area (OPA, sometimes referred to as the transverse occipital sulcus or TOS), whose scene-selective voxels are connected with scene-selective voxels in lingual, which in turn connect with parahippocampal (PPA). The second subnetwork includes precuneus, which contains the retrosplenial complex (RSC), lateral occipital and superior temporal cortices.

Discussion

We previously demonstrated that connectivity as measured by DWI is a powerful predictor of functional selectivity in the brain (Saygin et al. 2012; Osher et al. in prep). Here we assess the model coefficients from Osher et al. in prep, comparing the functionally-relevant networks (FRNs) across each of the four functional contrasts (faces, bodies, scenes, objects) for several key anatomical parcels that contain functionally-selective components (functional regions of interest, fROIs) across the contrasts.

We assessed both forward and reverse FRNs, the set of parcels that a particular region is predicted by or in turn predicts respectively. We observed there are unique connectivity patterns for the main occipitotemporal parcels that encapsulate the fROIs. Within the fusiform (containing FFA-faces; FBA-bodies; pFS-objects), the FRNs are highly similar between faces and bodies, while for objects they are vastly different. Face responses in fusiform and lateral occipital (OFA-faces; EBA-bodies; LOC-objects) are restricted to occipitotemporal predictors, and are in turn predictive of primarily occipitotemporal regions. Face-selectivity in the superior temporal sulcus (STS-faces) is also predicted by occipitotemporal regions but in turn predicts face-selectivity all across the cortex, including frontal regions. This may suggest that the STS is separate from the other components of the face network and is especially 'chatty' with the rest of the brain, and perhaps is responsible for projecting face information to more abstract association cortices. It will be interesting to compare these fingerprints to the representation of higher-order cognitive functions, such as language, memory, and theory-of mind.

Next, rather than comparing the FRNs across contrasts and within a region, we assessed the network of FRNs across regions for each contrast separately. Specifically, we analyzed the

subnetwork of occipitotemporal cortices, and focused our analyses to only the bidirectional and positive edges. The subnetworks of bidirectional positive edges are especially informative because they reflect a very specialized connectivity pattern: the voxels that most strongly connect these nodes are those that selectively respond to the given functional contrast. In other words, if connectivity between two regions is mutually positively predictive, it follows that the most functionally selective voxels are particularly connected to one another. By contrast, unidirectional positive edges reflect a connectivity pattern wherein functionally selective voxels of one region are diffusely connected to the other, regardless of that region's selectivity.

Negative edges are the most vague and difficult to interpret because they reflect connectivity patterns involving nonselective voxels, and although these voxels may be functionally similar in other domains, all we can deduce from this situation is that the connected voxels are not selective to the given contrast. Again, the subnetworks that we depict include only bidirectional positive edges as they are the most parsimonious components of the full network, and at present they are the easiest to interpret; it is important to keep in mind that these are subnetworks and that certainly other informative facets lay hiding in the complexity of the full network.

We found that there are parallel and interconnected pathways of information flow that are specific for certain functional categories. Face-selective voxels in the fusiform and lateral occipital were specifically connected to one another, as were bank of STS and superior temporal sulcus. However, face-selective voxels across these pairs were not specifically connected with one another. It is important to note that this result does not imply that these regions are not connected to one another (i.e. fusiform to superior temporal sulcus) or even that the face-selective voxels within these regions are not connected to one another. Rather this demonstrates

that FFA, OFA are not preferentially connected with banks STS and superior temporal sulcus, compared to the surrounding non-face-selective cortex. If one were to assess direct connectivity between the functional ROIs (rather than the anatomical ROIs as we do here), they may conclude that they are connected but this would ignore the specialization of these connections with respect to face-selectivity. In other words, fusiform and superior temporal sulcus may be heavily connected to one another as a whole, and so a limited fROI connectivity analysis would miss that this connectivity is not specialized for face-processing. Nonetheless, these results suggest that there are two face-processing streams, which was recently also proposed by Yovel and Friewald due to mounting comparative evidence from monkey and human studies alike (Yovel and Friewald 2013; Gschwind et al 2012).

For body and object processing, we observed a unique motif common to both FRN subnetworks, wherein selective voxels in lateral occipital are connected to fusiform via a three-way interaction through inferior temporal and inferior parietal cortex. This is especially intriguing because lateral occipital houses both EBA and LOC, while fusiform contains FBA and pFS. This result suggests that the information between these two regions is not necessarily directly relayed to one another but rather may undergo intermediate transformations through additional extrastriate cortices. Finally, we found that the FRN for scenes exists as two parallel subnetworks, one containing OPA and PPA and the other contains RSC. This is consistent with reports that RSC differs from other components of the scene-processing network in its representation of contextual information or gist (e.g. Park and Chun 2009).

Overall we show that specific connectivity patterns exist between functionally-selective voxels all the way from early visual areas through areas specialized in high-level vision. It will be important to expand this approach to retinotopic as well as higher-cognitive in order to

characterize the networks from early visual areas to higher-level cognitive regions.

References.

Park, S. and Chun, MM. Different roles of the parahippocampal place area (PPA) and retrosplenial cortex (RSC) in panoramic scene perception. Neuroimage 47(4). 1747. (2009).

Gschwind et al. White-Matter Connectivity between Face-Responsive Regions in the Human Brain. Cerebral Cortex 22:1564-1576. (2012).

Saygin, Z. M., Osher, D. E., Koldewyn, K., Reynolds, G., Gabrieli, J. D. E., & Saxe, R. R. (2012). Anatomical connectivity patterns predict face selectivity in the fusiform gyrus. Nat. Neurosci., 15(2), 321–7. doi:10.1038/nn.3001

Reese, T.G., Heid, O., Weisskoff, R.M. & Wedeen, V.J. Reduction of eddy-current-induced distortion in diffusion MRI using a twice-refocused spin echo. Magn. Reson. Med. 49, 177–182 (2003).

Galit Y., Freiwald, W. Face recognition systems in monkey and human: are they the same thing? F1000Prime reports, 5 (2013).

Fischl, B. et al. Automatically parcellating the human cerebral cortex. Cereb. Cortex 14, 11–22 (2004).

Fischl, B. et al. Whole brain segmentation: automated labeling of neuroanatomical structures in the human brain. Neuron 33, 341–355 (2002).

Desikan, R.S. et al. An automated labeling system for subdividing the human cerebral cortex on MRI scans into gyral based regions of interest. Neuroimage 31, 968–980 (2006).

Behrens, T.E., Berg, H.J., Jbabdi, S., Rushworth, M.F. & Woolrich, M.W. Probabilistic diffusion tractography with multiple fibre orientations: what can we gain? Neuroimage 34, 144–155 (2007).

Pitcher, D., Dilks, D.D., Saxe, R.R., Triantafyllou, C. & Kanwisher, N. Differential selectivity for dynamic versus static information in face-selective cortical regions. Neuroimage 56, 2356–2363 (2011).

Conclusions.

This research can encourage the assembly of a database of similar structure-function relationships (i.e. FRNs) for numerous other domains, in addition to the ones studied here. This would allow researchers to bridge the fingerprints across different brain regions and test mechanistic models of human brain function within and across different systems/networks.

Also, this method will enable researchers to estimate the functional responses to a range of experimental conditions in individual subjects with only a 10-minute diffusion scan. The more FRNs that can be accumulated in a shared database, the more a diffusion scan can tell us about an individual. In this thesis I showed that DWI connectivity can accurately predict activation across the brain and for various different functions in two different groups of participants and can thus be an alternative to group activation maps of function. The methodology used in this thesis will thus have important clinical applications, especially for pre-surgical planning. The identification of connectivity fingerprints for critical functions such as language could potentially empower surgeons to estimate relevant brain regions without the use of an fMRI scan and while the patient is asleep, or anesthetized. Finally, I intend to amass these datasets into a single Bayesian generative model, under which the probability of a particular functional response is conditioned on the set of probabilities of connecting to each parcel and the functional response of the connected voxels themselves. By doing so, we can take into account multiple functional domains, the responses of both connected components, and potentially individual differences into a single model. This would also allow us to discover what the optimal set of functional localizers to acquire on an individual subject, which will explain as much additional information as possible.